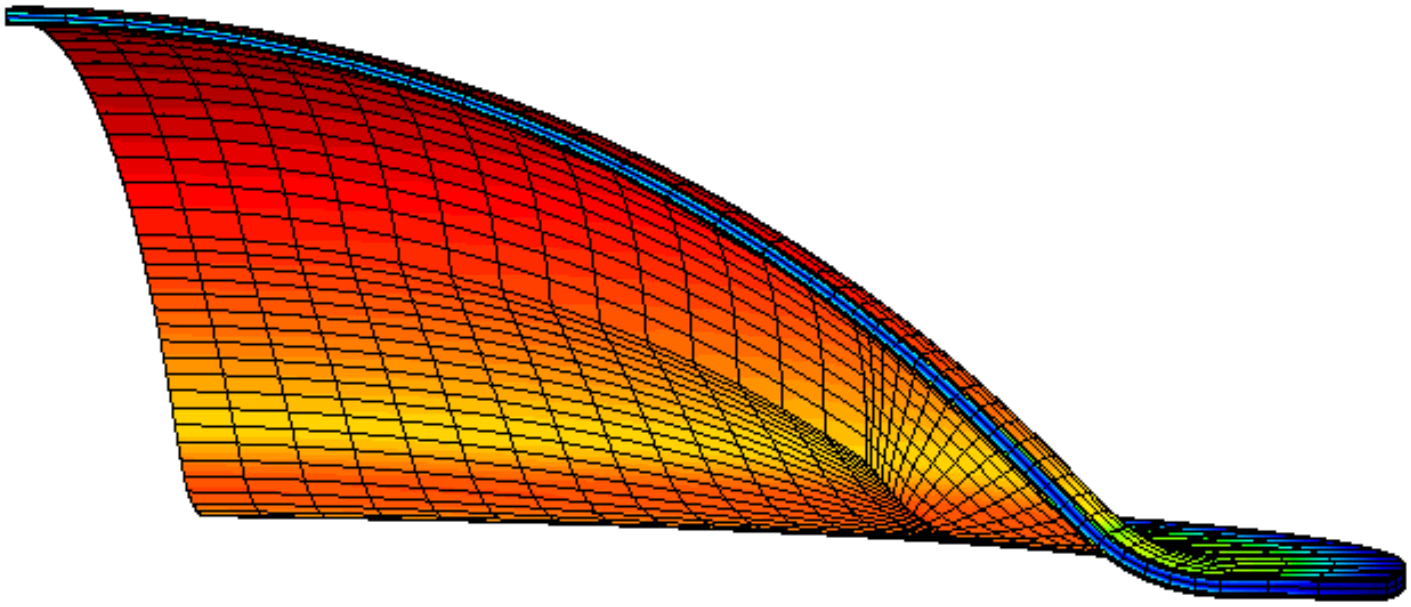

Tomás Mendonça Nicolau da Costa

Numerical study on the characterization of the plastic behaviour of multilayer sheets

Dissertação de Mestrado em Engenharia Mecânica
na Especialidade de Produção e Projeto

Julho/2018

· U C ·

Universidade de Coimbra

• U C •

FCTUC FACULDADE DE CIÊNCIAS
E TECNOLOGIA
UNIVERSIDADE DE COIMBRA

DEPARTAMENTO DE
ENGENHARIA MECÂNICA

Numerical study on the characterization of the plastic behaviour of multilayer sheets

Submitted in Partial Fulfilment of the Requirements for the Degree of Master in Mechanical Engineering in the speciality of Production and Project

Estudo numérico sobre a caracterização do comportamento plástico de chapas multicamada

Author

Tomás Mendonça Nicolau da Costa

Advisors

Pedro André Dias Prates

José Valdemar Bidarra Fernandes

Jury

President	**Professora Doutora Marta Cristina Cardoso de Oliveira** **Professora Auxiliar da Universidade de Coimbra**
Vowels	**Professor Doutor Abel Dias dos Santos** **Professor Associado da Faculdade de Engenharia da Universidade do Porto** **Mestre André Filipe Gomes Pereira** **Bolseiro de Doutoramento da Universidade de Coimbra**
Advisor	**Professor Doutor Pedro André Dias Prates** **Professor Auxiliar Convidado da Universidade de Coimbra**

Coimbra, July, 2018

“We are a product of those who taught us, who gave us an opportunity, who have given us chances, who’ve inspired us.”

Thomas Keller

Aos meus pais.

ACKNOWLEDGEMENTS

This dissertation represents, for the time being, the end of my academic path. Living and studying in Coimbra for six years made me grow a lot as a person and gave me some incredible moments that contributed for a wonderful experience overall. I am very happy and proud to finish this stage of my life and very excited about the future.

With that said, there's a few people I'd like to acknowledge, for without them, this would not have been possible.

I'd like to thank my advisors, Pedro Prates and Valdemar Fernandes for all their support and availability throughout the last semester. I'd like to extend that thank you note to all my colleagues at the Technology Group, where the atmosphere was always friendly and I could always rely on people for help.

Also, I want to thank my family. They were my cornerstone and supported me all the way, especially in the toughest times, for which I am extremely grateful.

Last but not least, a huge thank you to all my friends and the colleagues that I met over the last few years and who helped me in many ways and with whom I created many beautiful memories.

Thank you.

Abstract

Nowadays, composite materials are assuming an increasingly important role in material forming processes. They are popular because they can combine great physical and mechanical properties with a relatively low weight. Composites also have a very wide range of applications.

The main objective of this work is to study the plastic behaviour of multi-layer sheets and their formability. This was attained through finite element modelling that allowed numerical simulations, resorting to the in-house finite element code DD3IMP; the GiD software was used in the analysis of the results. In numerical simulations, the materials are considered isotropic, meaning that their behaviour is independent from the direction of the applied loading. Besides studying the plastic behaviour of multilayer sheets, another objective of this work is, if possible, to identify a material equivalent to the composite material, that is, a single material having a plastic behaviour similar to that of the composite.

The main object of this study is a three-layer sheet, composed by two outer layers of steel and a core made up of a polymeric material or an aluminium. The sheet is submitted to mechanical testing and forming processes, in order to characterize and understand the behaviour of composite materials. Both the sheet and the equivalent material were submitted to numerical simulations of the bulge test and also to the deep drawing of a U-channel profile and a square cup.

Keywords Composite materials, Multi-layer sheets, Equivalent material, Plastic behaviour, Numerical simulations, Forming processes

Resumo

Atualmente, os materiais compósitos estão a assumir um papel cada vez mais importante nos processos de conformação de materiais. São populares porque combinam excelentes propriedades físicas e mecânicas com um peso relativamente baixo. Além disso, os compósitos têm um vasto campo de aplicação.

O objetivo principal deste trabalho é estudar o comportamento plástico de chapas multicamada e a sua conformabilidade. Isto foi conseguido através de modelação por elementos finitos que permitiram a realização de simulações numéricas, recorrendo ao código de elementos finitos DD3IMP; o software GiD foi também usado na análise dos resultados. Nas simulações numéricas, os materiais são considerados isotrópicos, o que significa que o seu comportamento é independente da direção do carregamento aplicado. Além de estudar o comportamento plástico das chapas multicamada, outro objetivo deste trabalho passa por identificar, se possível, um material equivalente ao material compósito, ou seja, um material único que tenha um comportamento plástico semelhante ao do compósito.

O principal objeto deste estudo é uma chapa com três camadas, composta por duas camadas exteriores de aço, sendo o núcleo constituído por um material polimérico ou um alumínio. A chapa é submetida a um ensaio mecânico e processos de conformação plástica, por forma a caracterizar e compreender o comportamento de materiais compósitos. Tanto o compósito como o material equivalente foram sujeitos a simulações do ensaio de expansão biaxial sob pressão de óleo, bem como aos processos de estampagem de um perfil em U e de uma taça quadrada.

Palavras-chave: Materiais compósitos, Chapas multicamada, Material equivalente, Comportamento plástico, Simulações numéricas, Processos de conformação

Contents

LIST OF FIGURES

LIST OF TABLES

SYMBOLOGY

BHF – Blank holder force

E –Young's modulus

f – Punch-die clearance

h – Pole height

K – Strength coefficient (Swift Law)

n – Strain hardening exponent (Swift Law)

P – Pressure

r – Die radius

t – Sheet thickness

Y_0 – Yield stress

v - Poisson's ratio

$F(\mathbf{A})$ – Objective function

$\mathbf{A}$ – Vector of parameters $[Y_0\ K, n]$

q – Number of points

P^{exp} – pressure of reference experimental curve

P^{num} – pressure of numerical curve

h_i – pole height

R_M – die radius

R_1 – die profile radius

R_D – radius of central part of draw bead

R_S – initial blank radius of the circular sheet

ACRONYMS

DD3IMP – Deep Drawing 3D Implicit Finite Element Code

FEUP – Faculty of Engineering of the University of Porto

INEGI – Instituto de Ciência e Inovação em Engenharia Mecânica e Gestão Industrial

1. INTRODUCTION

Multi-layer sheets are composed of two or more layers, having become increasingly popular in the aerospace and automotive industries (Bagherzadeh et al., 2012). These can also be referred to as sandwich materials, which, as the name suggests, are materials typically composed of two outer layers, usually thin and with high rigidity, combined with a thicker, less rigid core, as schematically shown in Figure 1.1. Composite materials, such as multi-layer sheets, are highly sought-after because they can achieve similar performance when compared to traditional materials, combined with a reduced weight. This is especially important in the automotive industry, where the need for higher efficiency and lower emissions of greenhouse gases is ever increasing. Those needs can be achieved by reducing the weight of the car components.

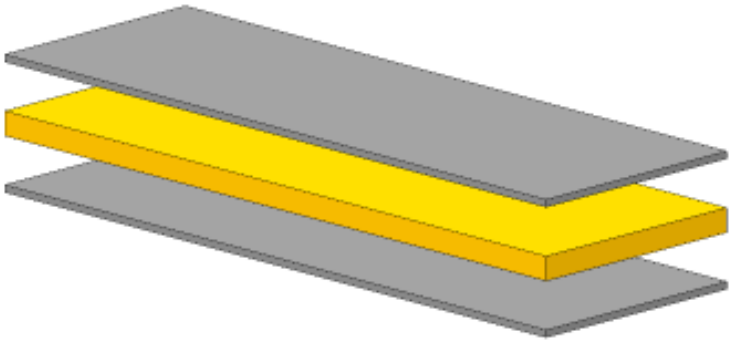

Figure 1.1. Schematic representation of a three-layer sheet, composed by two metal sheets and a polymeric core

The mechanical properties of multi-layer sheets are governed by the volume fractions and material properties of each layer, leading to desirable features such as low weight, high mechanical resistance, ductility, corrosion resistance and good thermal and electrical properties simultaneously (Marandi et al., 2017). The materials of multi-layer sheets can be bonded together by manufacturing methods such as explosive welding method (Marandi et al., 2017), cold and hot rolling (Bagherzadeh et al., 2012; Kim et al., 2017; Marandi et al., 2017) and adhesive bond (Bagherzadeh et al., 2012). In this context, poor

manufacturing of multilayer sheets, strong dissimilarity on the mechanical behaviour between layers and/or the volume fraction of each layer may lead to a number of failure modes, namely under bending solicitations. Examples of failure modes include: (i) delamination, i.e. separation between layers that occurs when the bond is relatively weak; (ii) skin wrinkling in the outer layer under compressive loading; (iii) outer layer failure, under tensile or compressive loading and (iv) core failure, due to shear stresses (Andrews and Moussa, 2009). In this regard, it becomes crucial to investigate the mechanical properties and suitability of multilayer metal sheets in forming processes, such as deep-drawing, which involve large plastic deformations.

A number of studies on the formability and mechanical behaviour of composite sheets can be found in the literature. For example, an extensive investigation on the formability of metal-polymer-metal sandwich sheets, with and without metal reinforcements, has been performed under stretching, bending and deep-drawing solicitations (Sokolova et al., 2011; Harhash et al., 2014; Harhash et al., 2017). In another study, the mechanical properties and plastic behaviour were investigated for a metal-polymer-metal composite sheet (Miranda et al., 2017). Uniaxial tensile tests were performed for characterizing the mechanical behaviour of the composite sheet and the outer metal layers; the plastic behaviour of the polymeric core was inferred by decomposition of the total load of the composite material. The hydraulic bulge test with a circular die was also performed for the mechanical characterization of the composite sheet and the outer metal layers up to large plastic strain values. The authors remark that the biaxial stress-strain curve of the composite material cannot be obtained from the direct use of the membrane theory, due to through-thickness inhomogeneity of the sheet.

In this dissertation, a numerical simulation study is carried out with the aim of evaluating the forming capability of multi-layer sheets. Firstly, numerical simulations of the circular bulge test were performed for two three-layer sheets (composed by two outer layers of one material and a core made up of another material), in order to characterize and understand the behaviour of such composite materials. From this study, equivalent materials (i.e. single sheet materials having a plastic behaviour similar to that of the composite) were proposed for each composite material. Afterwards, numerical simulations of two types of deep-drawing tests, the U-channel profile and square cup tests, were carried out for both

composite materials and corresponding equivalent materials, to understand the specific forming characteristics of the composite materials.

1.1. Dissertation overview

This dissertation is organized in five chapters. For a better reading and orientation, this section briefly summarizes the content of the chapters.

Chapter 1 introduces the subject and the motivation for its study.

Chapter 2 presents an analysis on the plastic behaviour of two composite materials, supported by numerical simulation results of the circular bulge test and inverse analysis; an equivalency between single material sheets and composite sheets is established.

Chapters 3 and 4 present the numerical simulation study involving the U-channel profile and square cup forming tests, respectively.

Chapter 5 presents the main conclusions regarding the results analysed in the previous chapters, and suggestions for future work.

2. BULGE TEST

2.1. Numerical modelling

The geometry of the tools considered in the test is schematically shown in Figure 2.1, where R_M=75 mm is the die radius, R_1=13 mm is the die profile radius, R_D=95 mm is the radius of the central part of the draw bead and R_S=100 mm is the initial blank radius of the circular sheet. This geometry was built based on the experimental bulge test used by Santos et al. (2010). The tools were described using Bézier surfaces, considering only one quarter of the geometry due to the material and geometrical symmetry conditions. However, in order to simplify the analysis, the draw bead geometry was neglected and its effect was replaced by a boundary condition imposing radial restriction on the displacement of the nodes placed at a distance equal to R_D from the centre of the circular sheet. The numerical simulations were carried out with the DD3IMP (Deep Drawing 3D Implicit Finite Element Code) in-house code assuming an incremental increase of the pressure applied to the inner surface of the sheet. The constitutive model adopted for the finite element analysis assumes that: (i) the elastic behaviour is isotropic and described by the generalised Hooke's law; (ii) the plastic behaviour is described by the von Mises yield criterion and the hardening model by the Swift isotropic law. The contact with friction was described by the Coulomb law with a friction coefficient of 0.02.

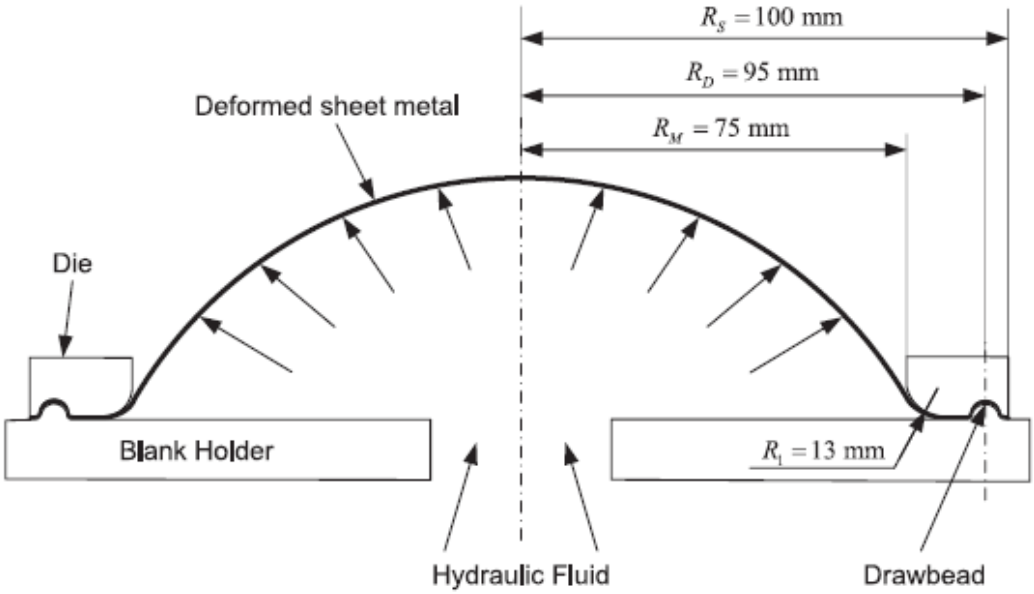

Figure 2.1. Schematic representation of the bulge test, with identification of the main dimensions

The blank sheet, 1.6 mm thick, was discretized with hexahedral solid elements, using two layers of elements for each layer of material, that is, six elements in total across the thickness.

A mesh sensitivity analysis was performed to examine the effects of the mesh discretization in the sheet plane on the results of the pressure *vs.* pole height. A good compromise between the results and the simulation time was achieved for the mesh shown in Figure 2.2. This mesh was made up of 5490 hexahedral elements. On average, each simulation took around 1 hour to run.

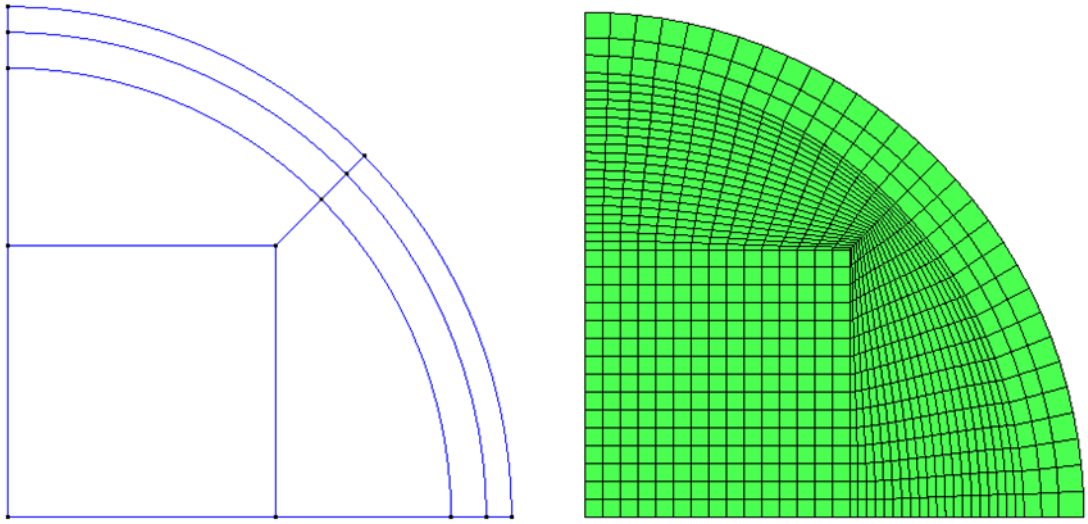

Figure 2.2. (a) Different areas used in discretization; (b) Final mesh used for the simulations

The simulations of the bulge test consisted of two phases. In phase one, the die applies pressure against the blank holder to hold the sheet in place. In phase two, pressure starts to be applied under the sheet and is incrementally increased.

2.2. Identification of parameters

The starting point for this work was an experimental study conducted by the Institute of Science and Innovation in Mechanical Engineering and Industrial Engineering (INEGI), Faculty of Engineering of the University of Porto (FEUP) and Inapal Metal SA (Miranda et al., 2017). Among others, it contains the experimental curves obtained in tensile and bulge tests of both a hybrid material with two outer layers of steel and a polymer core, with a 1.6 mm thickness, and the two outer layers of steel, with a combined thickness of 0.6 mm. Figure 2.3 shows the pressure *vs.* pole height curves of the bulge test.

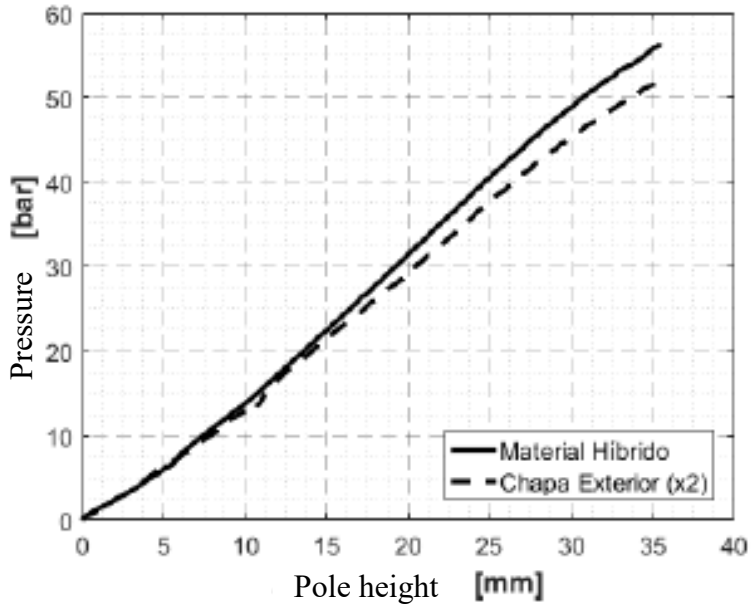

Figure 2.3. Reference experimental curves pressure *vs.* pole height of the hybrid material (solid line) and of the two outer layers of steel (dashed line) (Miranda et al., 2017)

These curves allowed to determine the constitutive parameters of the Swift law of the hybrid material and its constituent materials (the polymer and the metal), by inverse analysis. The following steps were performed:

(i) Using the application Web Plot Digitizer to obtain an excel file with the data points, from the curves in Figure 2.3.

(ii) Identification of the hardening parameters of the outer layers of steel. This consists of minimising the differences between the reference experimental and numerical curves of pressure vs. pole height. The minimization is performed by using the Levenberg-Marquardt algorithm, with the following objective least squares function $F(\mathbf{A})$:

$$F(\mathbf{A}) = \left(\frac{1}{q}\right) \sum_{i=1}^{q} \left(P^{exp}(h_i) - P^{num}(h_i)\right)^2 \quad (2.1)$$

where $\mathbf{A} = [Y_0, K, n]$ is the vector of parameters to be optimized; $P^{\mathrm{num}}(h_i)$ and $P^{\mathrm{exp}}(h_i)$ are respectively the numerical and reference values of the pressure for a given value of pole height, h_i; and q is the number of points. Polynomial interpolation is used to assess the numerical and reference

experimental pressure values for the same values of pole height, h_i. A total of 1000 points, uniformly distributed over the range of pole heights between 5 and 35 mm were used. The identification ends when the differences between the numerical and reference experimental values of pressure are such that $F(\mathbf{A}) \leq 6\text{x}10^{-4}$ MPa. Four iterations were carried out until reaching this value.

Figure 2.4 illustrates the comparison between the reference experimental curve of the outer layers of steel and the optimized. The input elastic parameters of all simulations were: Young's modulus, E = 210 GPa and Poisson´s ratio, $\nu = 0.30$. The input plastic parameters for the first estimate were equal to those obtained from the tensile test, as shown in Table 2.1. This table also shows the optimized parameters. From this point on, the properties of the steel were fixed for all simulations.

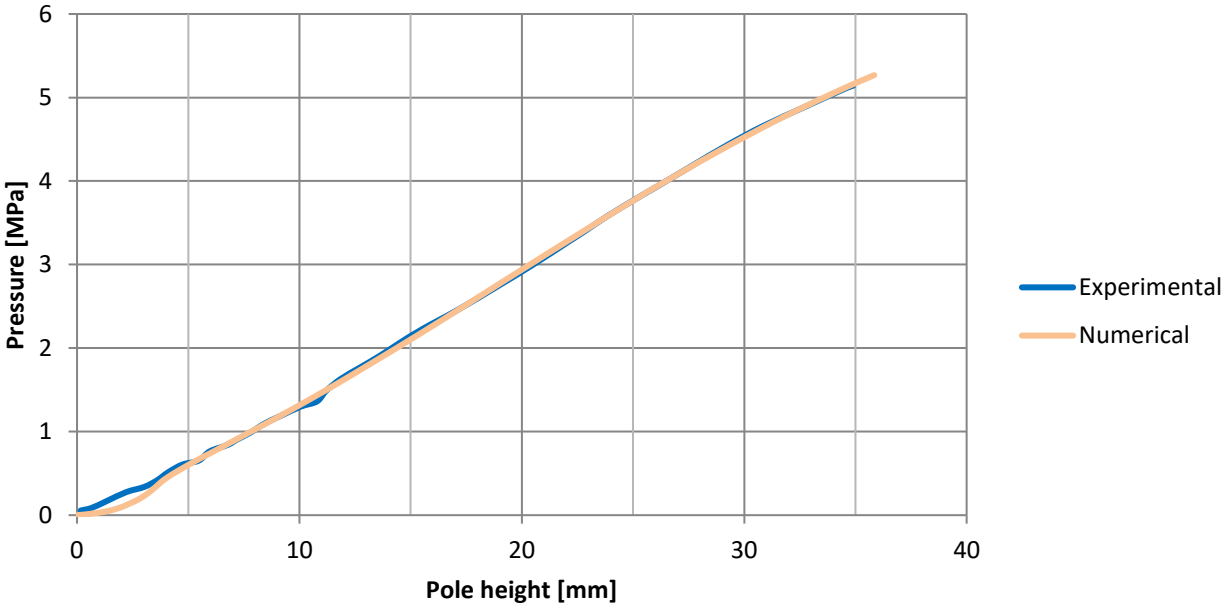

Figure 2.4. Comparison of the reference experimental pressure *vs.* pole height curve of the steel layers with the numerical curve obtained by optimization

(iii) Identification of the hardening parameters of the polymer core. In this case, the identification only concerns the value of the parameter K of the Swift law. In fact, the tensile curve of the polymer is rather horizontal (the hardening coefficient was fixed at the value n = 0.01) and the value of the yield stress fixed at Y_0 = 11.8 MPa, as indicated by Miranda et al. (2017). That is, only

the value of the parameter K of the Swift law was optimized. The inverse identification uses the pressure vs. pole height curve of the hybrid material and the procedure as above indicated in step (ii). Also, the Swift parameters of the outer layers of steel were kept fixed (see values in Table 2.1). Figure 2.5 illustrates the comparison between the reference experimental curve of the hybrid material and two numerical curves, the first estimate and the optimized. The input elastic parameters of the polymer core for all simulations were: Young's modulus, E = 0.98 GPa and Poisson ratio, ν = 0.38. Table 2.1 shows the input plastic parameters for the first and the optimized estimates (only K was optimized). Three iterations were needed to reach $F(\mathbf{A}) = 5.3\text{x}10^{-4}$ MPa

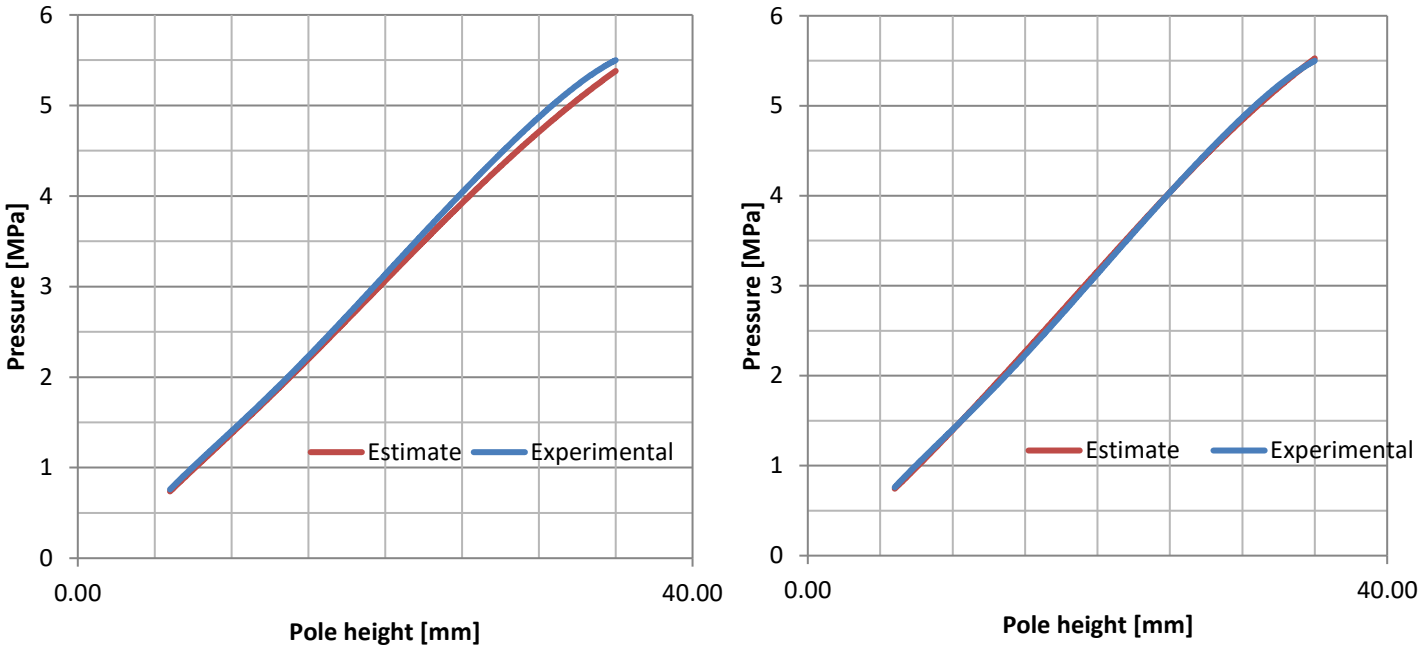

Figure 2.5. Comparison between the reference experimental curve of the hybrid material and: (a) initial estimate; (b) after optimization

The possibility of obtaining the pressure vs. pole height curve of the polymer from the difference between the curves corresponding to the composite and to the outer layers of steel is now analysed. That is, the follow equation is tested:

$$P_{polimer}(h_i) = P_{composite}(h_i) - P_{steel\ layers}(h_i) \qquad (2.2)$$

Table 2.1. Elastic and plastic parameters of the polymer core; only the parameter *K* was optimized. The elastic and plastic (identified) parameters of the outer layers of steel are also shown

	Materials	E	v	K	Y_0	n
First estimate	Inner layer	0.98 GPa	0.38	11.8 MPa	11.8 MPa	0.01
	Outer layers	210.0 GPa	0.30	747.04 MPa	339.6 MPa	0.188
Optimized	Inner layer	0.98 GPa	0.38	22.45 MPa	11.8 MPa	0.01
	Outer layers	210.0 GPa	0.30	858.7 MPa	382.5 MPa	0.239

Figure 2.6 shows the comparison between the curves obtained using the above equation, from the experimental and numerical results and numerically obtained using the identified parameters of the polymer shown in Table 2.1. Some differences occur between the three curves, although it is not possible to understand if the associated error can explain these differences.

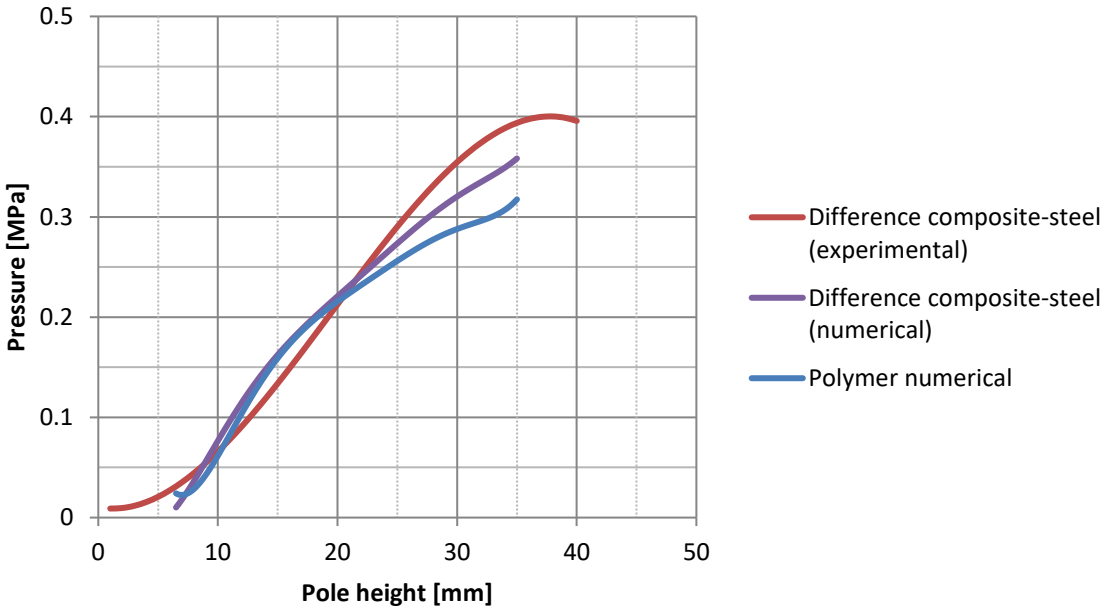

Figure 2.6. Comparison between pressure *vs.* pole height curves obtained as indicated to the right of the figure

In order to clarify this, a new hybrid material was used such that the hardening curve of the core material has a higher level. This hybrid material has the outer layers with the same behaviour as the case above, although with a different core, whose behaviour is typical of an aluminium alloy. This new hybrid material will be referred to as composite 2 and the first one, with the polymeric core, will be referred to as composite 1.

The elastic and plastic properties assigned to components of the materials of the composite 2 are indicated in Table 2.2.

Table 2.2. Elastic and plastic parameters of the materials of the composite 2

Materials	E	v	K	Y_0	n
Outer layers	210.0 GPa	0.30	858.7 MPa	382.5 MPa	0.239
Inner layer	79.4 GPa	0.32	540.0 MPa	243.0 MPa	0.190

Figure 2.7 allows comparing of the mechanical behaviour of the constitutive materials of composites 1 and 2.

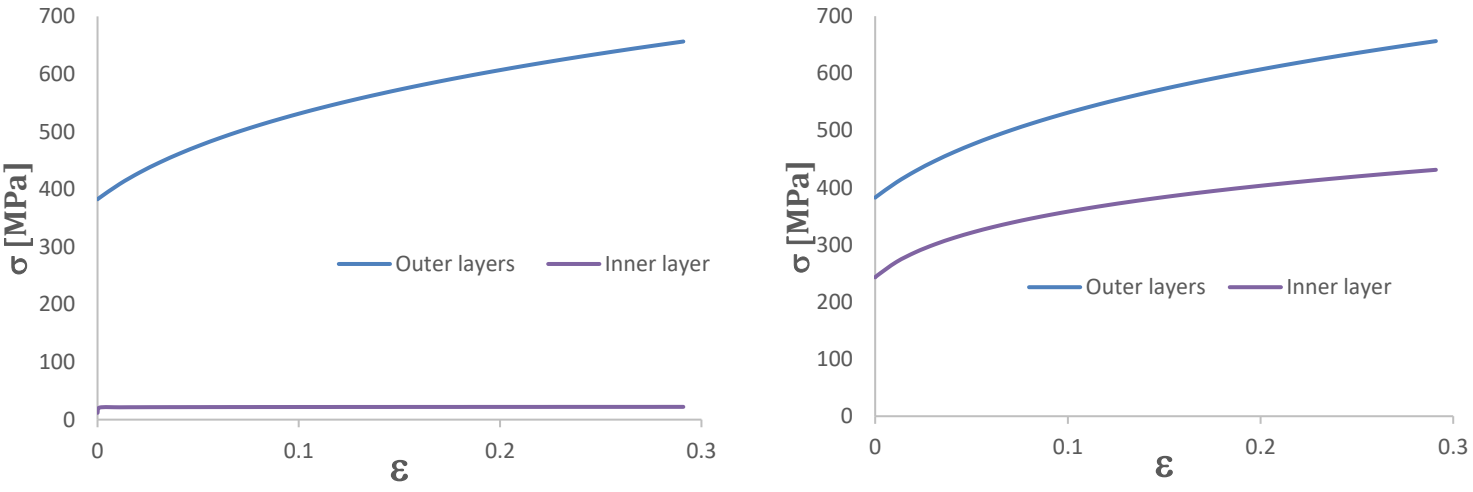

Figure 2.7. Stress-strain curves of the constitutive materials of: (a) composite 1; (b) composite 2

Numerical simulations were carried out with the same conditions and meshes as for composite 1. The simulations concern the core of aluminium alloy and the hybrid material; the results of the outer layers of steel are already known. Figure 2.8 shows the corresponding pressure vs. pole height curves. It is also shown the curve obtained by adding the curves of the two materials that make up the composite:

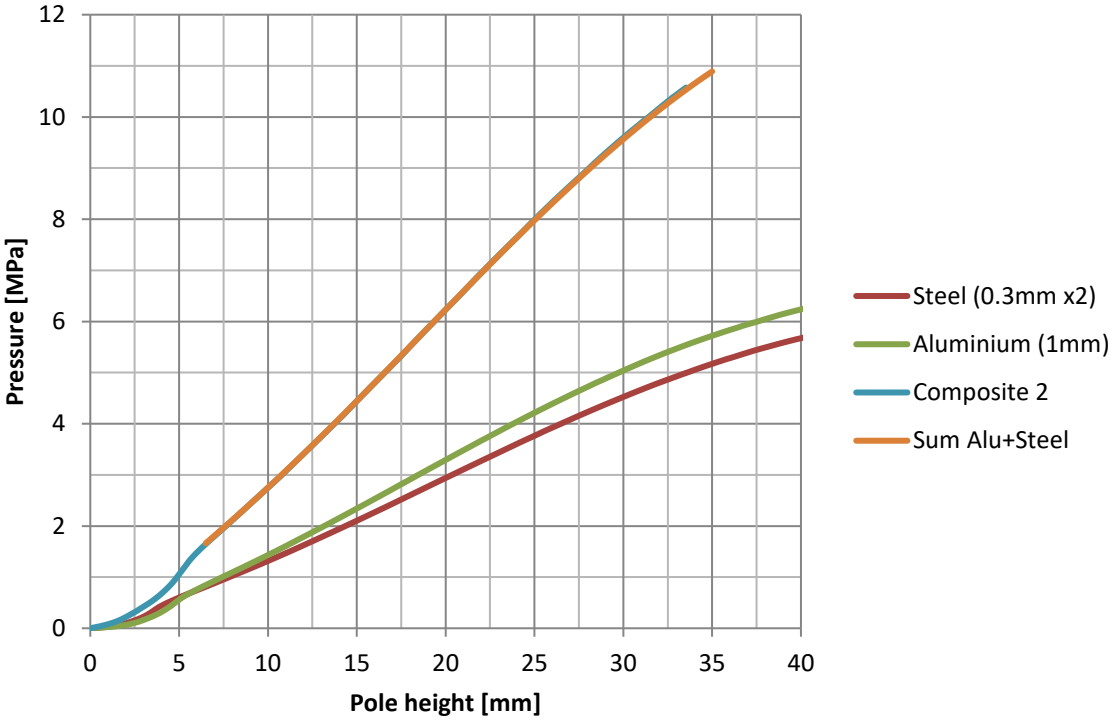

Figure 2.8. Composite 2: pressure *vs.* pole height curves of the composite and the materials of the outer and inner layers; the resulting curve of the sum of those of the individual layers is also shown.

It can be concluded that the sum of the curves of the inner and outer layers is equal to that of the composite material.

2.3. Equivalent Material

Now, an equivalent sheet consisting of a single material having the same thickness and behaviour of the composite material is considered. The Swift law parameters of this equivalent material were identified from the pressure vs. pole height curves of the

composites 1 and 2, using the inverse analysis procedure described in section 2.2. The elastic parameters of the equivalent material, used as input in the numerical simulations, were considered as the weighted average of the parameters of the materials of each composite. Table 2.3 shows these parameters and identification results of the Swift law parameters. Figure 2.9 show the overlap between the pressure vs. pole height curves of the composites and those of the corresponding equivalent materials.

Results similar to those of Table 2.3 are obtained when using the rule of mixtures for calculating the hardening curve of the equivalent material from the corresponding curves of the inner and outer layers materials. The weighted average of both hardening curves is used, such as for the elastic parameters. A fitting of the Swift curve is then carried out, using the Excel Solver.

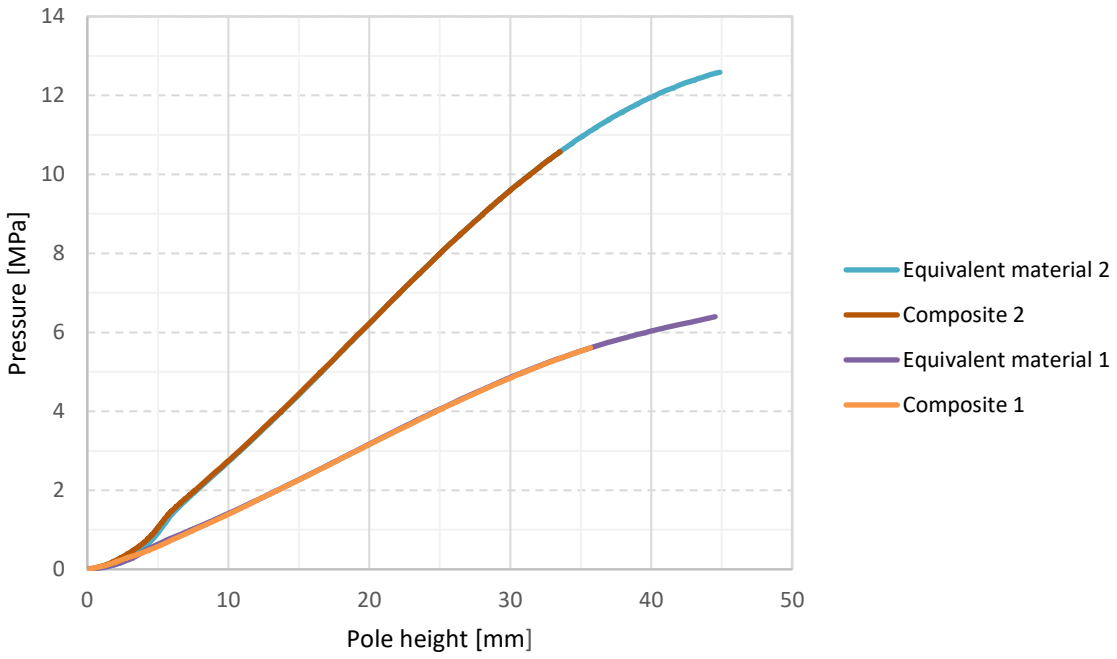

Figure 2.9. Comparison between the pressure *vs.* pole height curves of the two composites and the respective equivalent materials

Table 2.3. Elastic parameters and identified plastic parameters obtained for the equivalent materials of composites 1 and 2

Equiv. Material	E	v	K	Y_0	n
1	58.0 GPa	0.36	331.5 MPa	151.7 MPa	0.211
2	115.0 GPa	0.31	658.0 MPa	295.7 MPa	0.21

Later in this text, it will be analysed to what extent the concept of equivalent material can be applicable to other sheet forming processes.

2.4. Strain and stress distributions near the pole of the cup

This subchapter aims to analyse the strain and stress distributions in the sheet, for the composites and the corresponding equivalent materials. Figure 2.10 shows GiD images of the strain distribution of the composite 1 and the equivalent material.

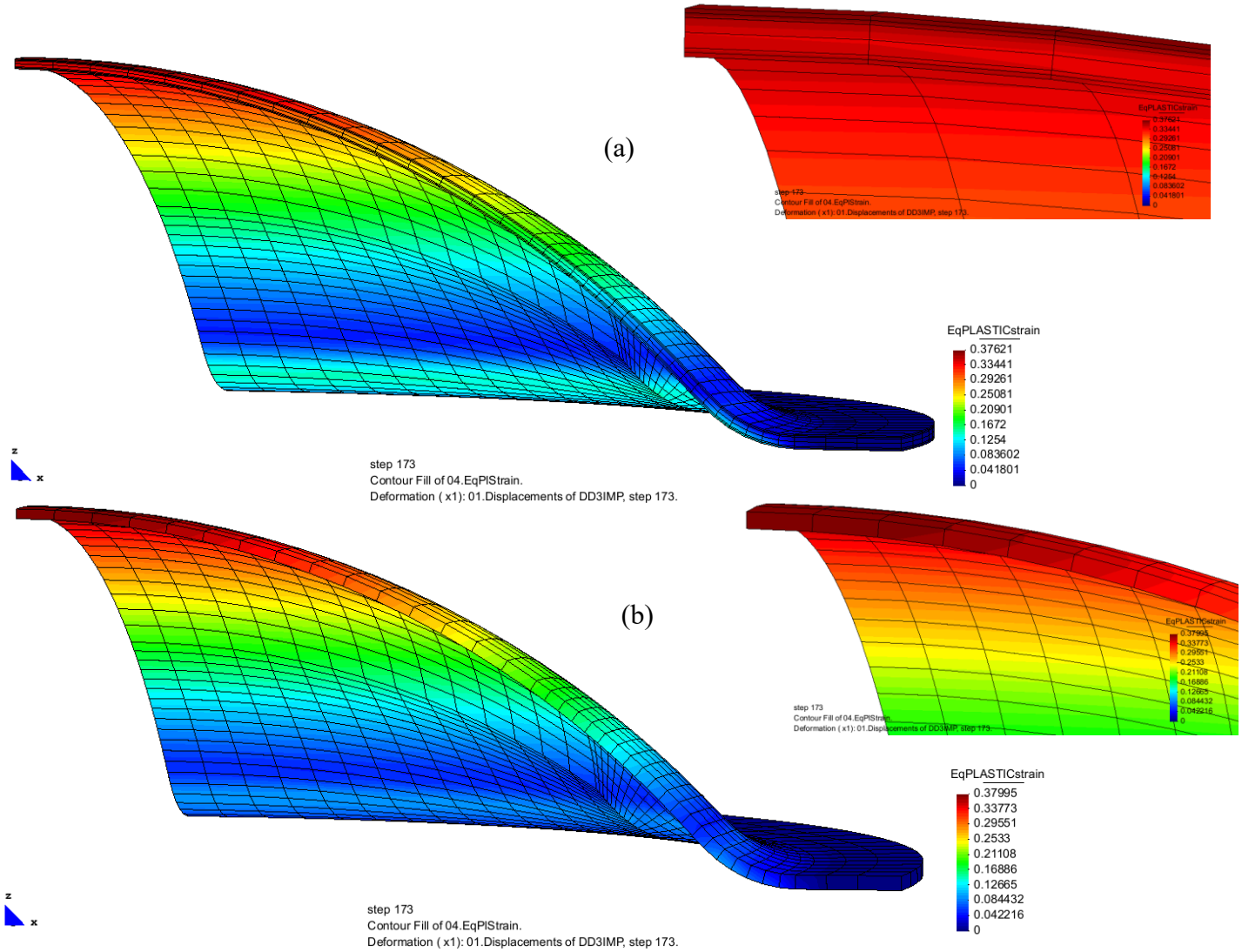

Figure 2.10. Distribution of equivalent plastic strain at the end of the test of the: (a) composite 1; (b) equivalent material 1

Although the strain in the composite is slightly higher than in the equivalent material, the maximum values of the equivalent plastic strains are very similar in both cases and about 38%.

Figure 2.11 displays the stress distributions of the sheets. In Figure 2.11 (a), the composite is represented and Figure 2.11 (b) shows the results of the equivalent material. As can be seen by the blue-ish colours, there is a huge stress gradient in thickness. This is particularly evident in the pole region, where the stress drops from around 690 MPa, in the outer sheets, to almost zero, at the middle point of the core.

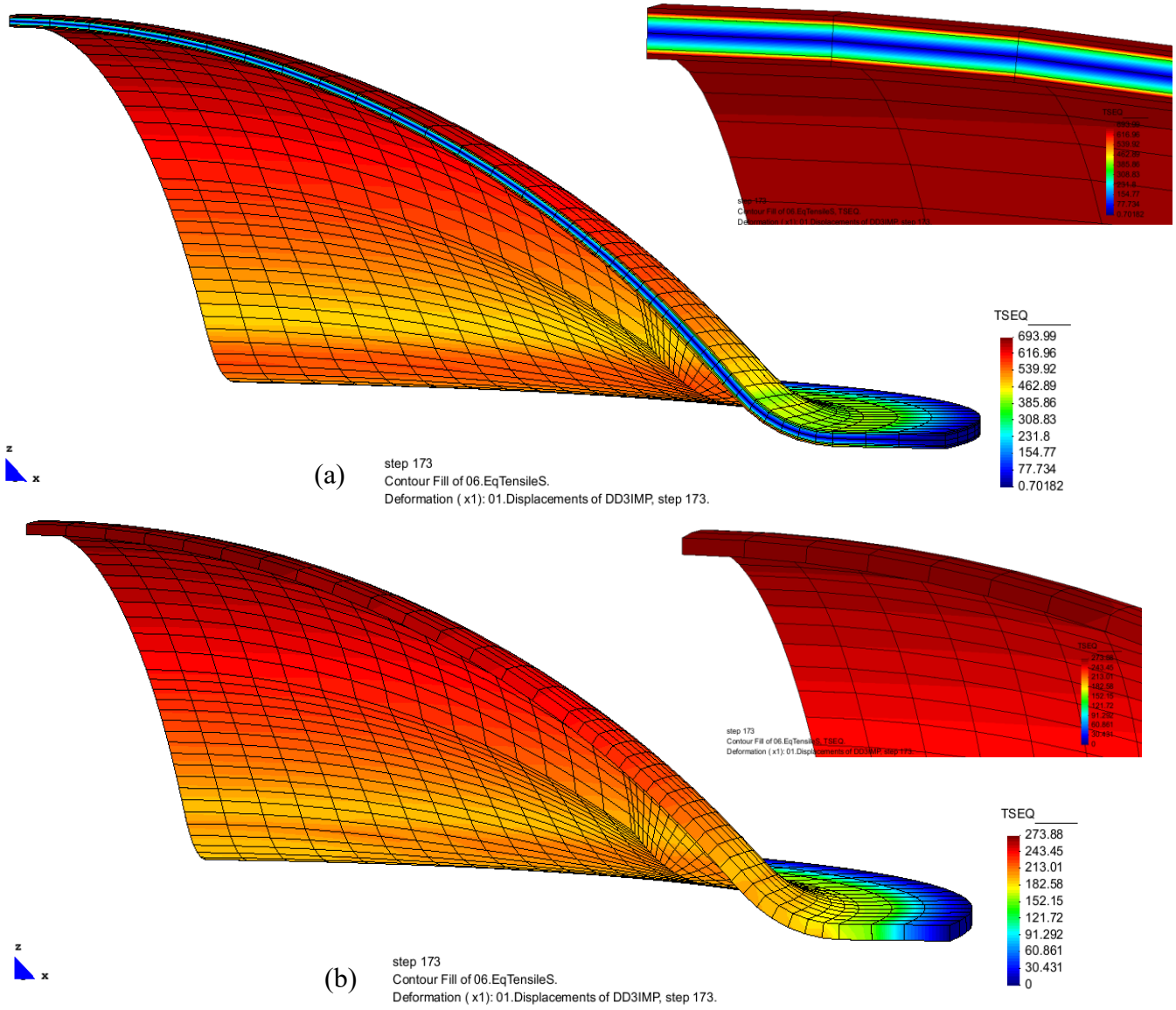

Figure 2.11. Distribution of equivalent stress at the end of the test of the: (a) composite 1; (b) equivalent material 1

Regarding the equivalent material, the maximum value of the stress is 273.88 MPa at the pole, which is far from the maximum stress in the composite.

The equivalent material seems to well replicate the behaviour of the composite in relation to the equivalent plastic strain; consequently, there are substantial differences between both materials with regard to equivalent stress.

3. DEEP DRAWING OF A U-CHANNEL PROFILE

Numerical simulations of U-channel forming process were performed, in order to compare the behaviours of the two-layered sheets and the previously defined equivalent sheets. The aim is to understand the specific forming characteristics of the three-layered materials. The choice fell on the forming of a U-channel profile because it is one of the most common and representative processes in the industry in sheet metal stamping.

Figure 3.1 schematically represents half of the typical setup for a deep drawing process of the U-channel profile, indicating the dimensions (mm) of the tools.

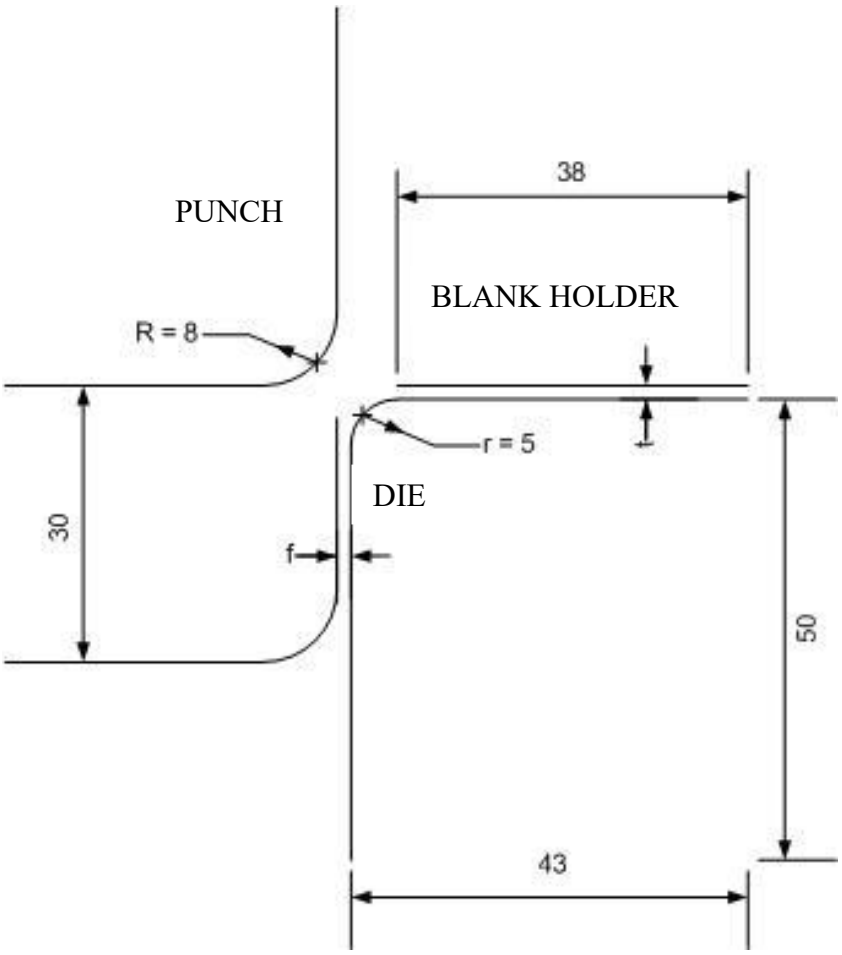

Figure 3.1. Schematic representation of the tool configuration for the deep drawing of the U-channel profile

3.1. Numerical modelling

The sheet with the initial dimensions of 75x35mm, with 1.6mm thickness, was discretized with just one element across the width and 150 elements across the length. Similarly to the mesh used for the bulge test, this mesh had 6 layers (two layers for each material) of elements across the thickness. Therefore, the mesh is composed of 900 hexahedral elements. Due to material and geometry symmetries, only one-half of the U-channel forming process was simulated; moreover, the boundary conditions impose a plane strain state, with null deformation along the width direction (0y axis in Fig. 3.2). The numerical simulations were carried out with the DD3IMP in-house code assuming an incremental increase of the punch displacement. The constitutive model is adopted under the same assumptions as for the bulge test. The contact with friction was described by the Coulomb law with a friction coefficient of 0.144 (Prates et al., 2018).

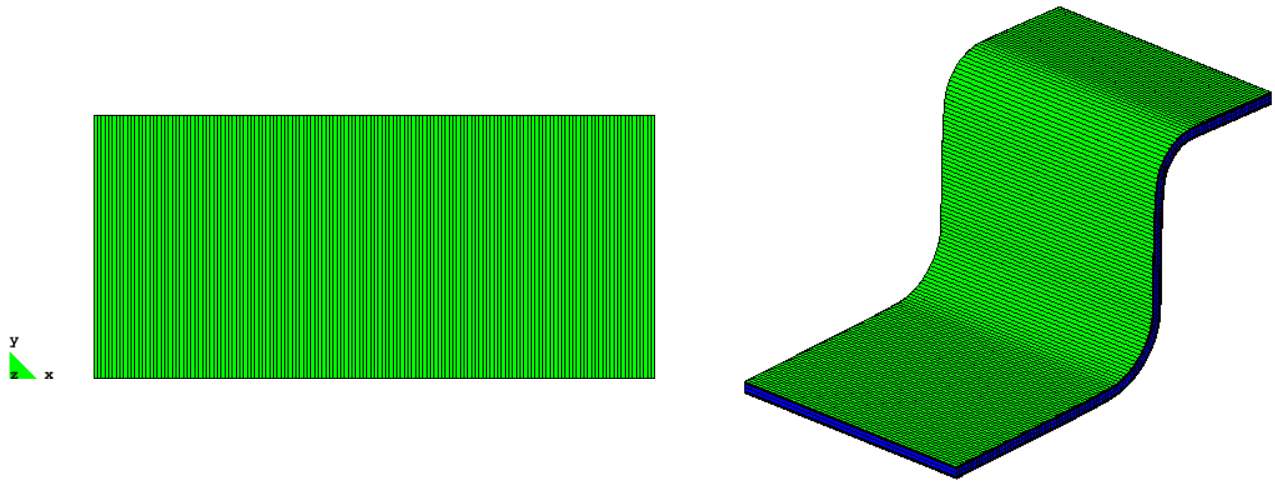

Figure 3.2. (a) Mesh viewed from the top; (b) Deformed mesh

Different combinations of process parameters were tested, concerning the blank holder force, die radius, sheet thickness and clearance between the punch and the die.

The different parameters used are:

Blank holder force (BHF):

- 4.9kN
- 19.6kN

Die radius (r):

- 5mm
- 8mm

Sheet thickness (t):

- 1.2mm
- 1.6mm

Punch-die clearance (f):

- 1.5mm (lower than sheet thickness)
- 1.6mm (equal to sheet thickness)
- 1.8mm (higher than sheet thickness)

The simulation of this deep drawing process is composed of two phases. In phase one, the blank holder compresses the sheet against the die. In phase two, force is applied to the punch until it travels 30mm along the negative direction of the z axis (Figure 3.2 (a)).

The focus of the analysis is the deformation in sheet thickness. Also, the force *vs.* displacement results will be analysed to assess the behaviour of the equivalent materials when compared to the respective composites.

3.2. Strain distributions analysis

The results of the strain distributions of the two composites are presented and compared with those of the equivalent materials.

3.2.1. Composite 1

Table 3.1 provides an overview of the different combinations of parameters used for the simulations of composite 1.

Table 3.1. Combination of parameters used for the simulations of composite 1

Case	BHF [kN]	r [mm]	t [mm]	f [mm]
A	4.9	5	1.6	1.6
B	19.6	5	1.6	1.6
C	19.6	5	1.6	1.5
D	19.6	5	1.6	1.8
E	19.6	8	1.6	1.6
F	19.6	5	1.2	1.2
G	19.6	8	1.2	1.2

The first simulation was run with BHF = 4.9 kN (Case A). The results of the equivalent plastic strain at the end of the forming process are shown in Figure 3.3 (a). The strong difference of mechanical behaviour between the materials of the composite 1, produces a strong strain gradient in the composite, with high strain values in the half of the core, on the side of the die. This does not occur in case of the corresponding equivalent material, as shown in Figure 3.3 (b), for which the maximum strain attained is at about two and a half times smaller than in the composite.

In order to test to what extent the process parameters influence the strain distribution, it was firstly decided to increase the value of BHF and then change other process parameters such as the die radius and the clearance. Figure 3.4 (a) shows the case of BHF = 19.6 kN (Case B). It can be concluded that the increase in the blank holder force led to a decrease in the maximum value of equivalent plastic strain of around 32%, and consequent reduction of the strain gradient. In contrast, the equivalent material exhibits a strain distribution almost identical to that of the previous case (equivalent material 1), in particular the equivalent maximum strain is not quite different.

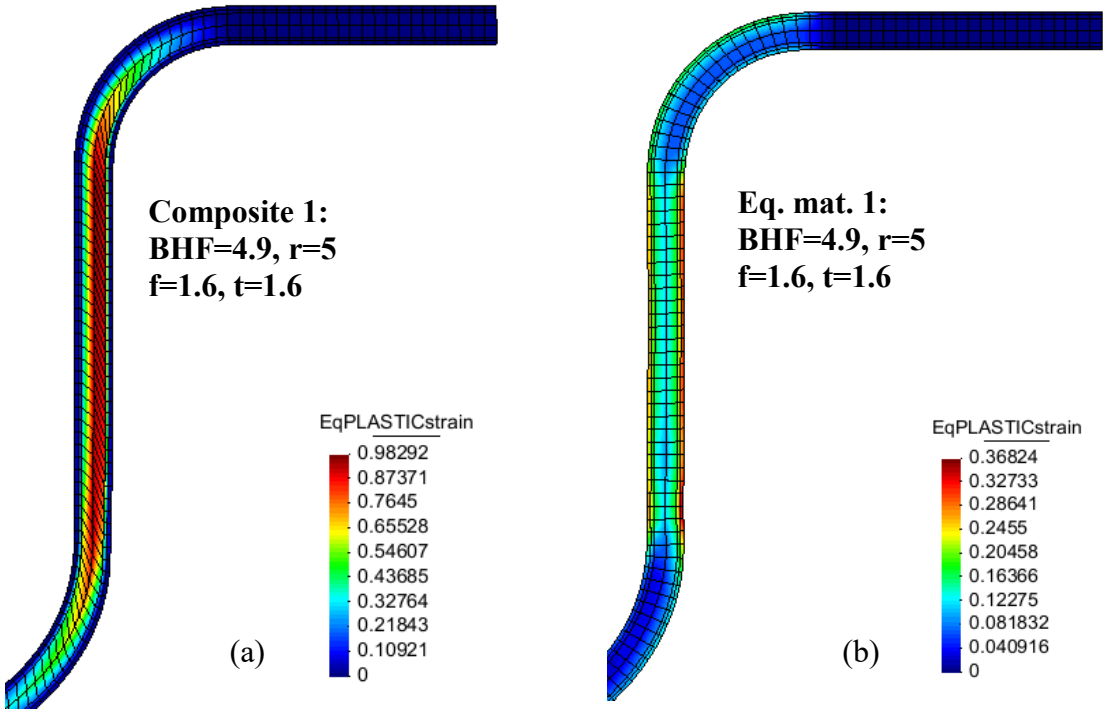

Figure 3.3. Distribution of equivalent plastic strain at the end of the forming process (Case A): (a) composite 1; (b) Equivalent material 1

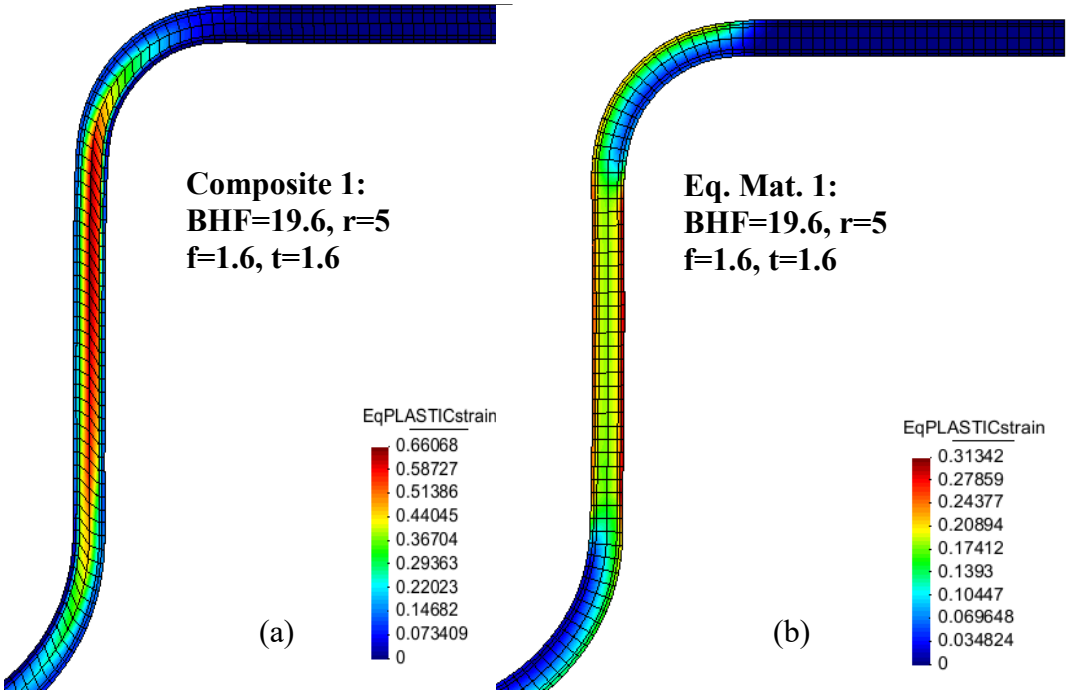

Figure 3.4. Distribution of equivalent plastic strain at the end of the forming process (Case B): (a) composite 1; (b) Equivalent material 1

In the previous two cases, the clearance is equal to the thickness of the sheet. Now, two other clearance values are used, one lower (Case C in Figure 3.5(a)) and one higher (Case D in Figure 3.5(b)) than the sheet thickness. The results shows that in both cases the equivalent plastic strain is slightly higher than in Case B. That is, the clearance between the punch and the die does not have a significant effect on the results.

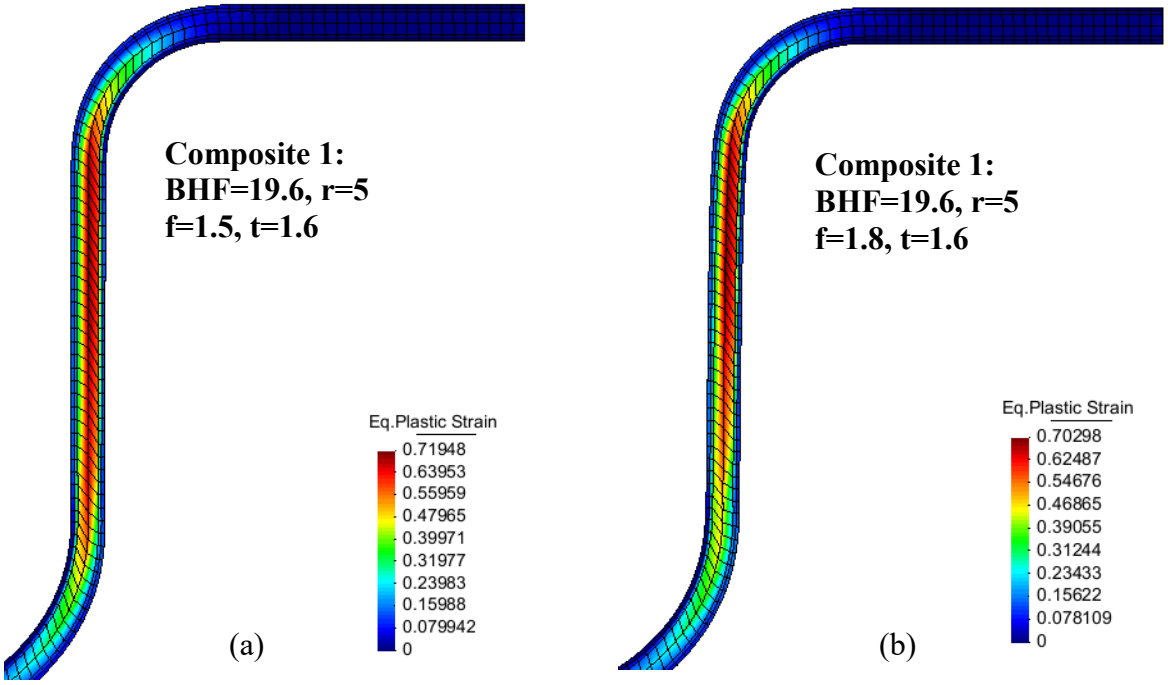

Figure 3.5. Distribution of equivalent plastic strain at the end of the forming process of the composite 1: (a) Case C; (b) Case D

Figure 3.6 (a) shows that the strain gradient is reduced for smoother die geometries. In this figure, the die radius was increased from 5 mm to 8 mm (Case E), in order to match the punch radius. The results show that the maximum value of the equivalent strain is strongly reduced relative to the previous cases, and thus also the gradient is reduced. Although the maximum value of the equivalent strain remains higher than that of the equivalent material, as shown in Figure 3.6 (b), it is already similar to those of the equivalent material with the radius of 5 mm (Figure 3.4 (b)).

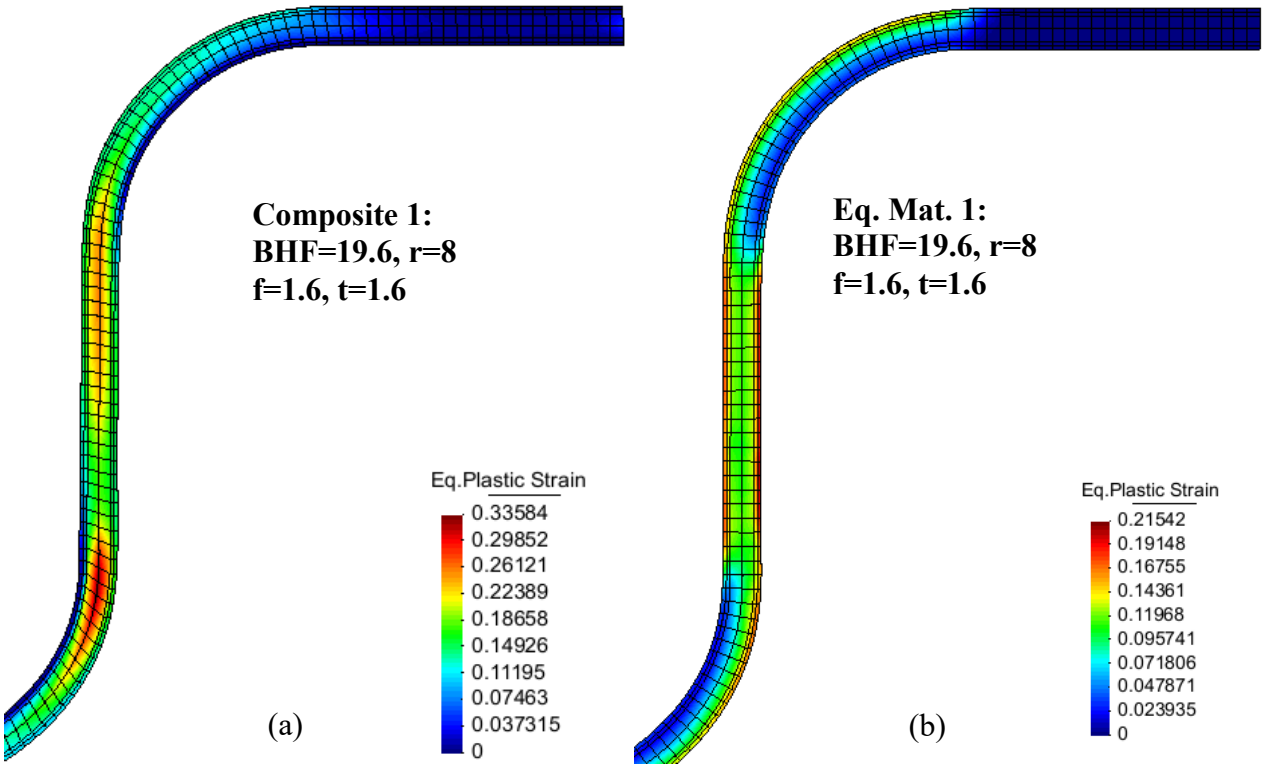

Figure 3.6. Distribution of equivalent plastic strain at the end of the forming process (Case E): (a) composite 1; (b) Equivalent material 1

Thus, it can be concluded that the optimum conditions for this process with composite 1 are BHF = 19.6kN, a clearance equal to the thickness of the sheet, and a die radius of 8 mm. Otherwise, the strong strain gradients can cause failure by delamination, which was observed to strongly depend on the geometric conditions, in the case of the three-point-bending test (Sokolova et al., 2011).

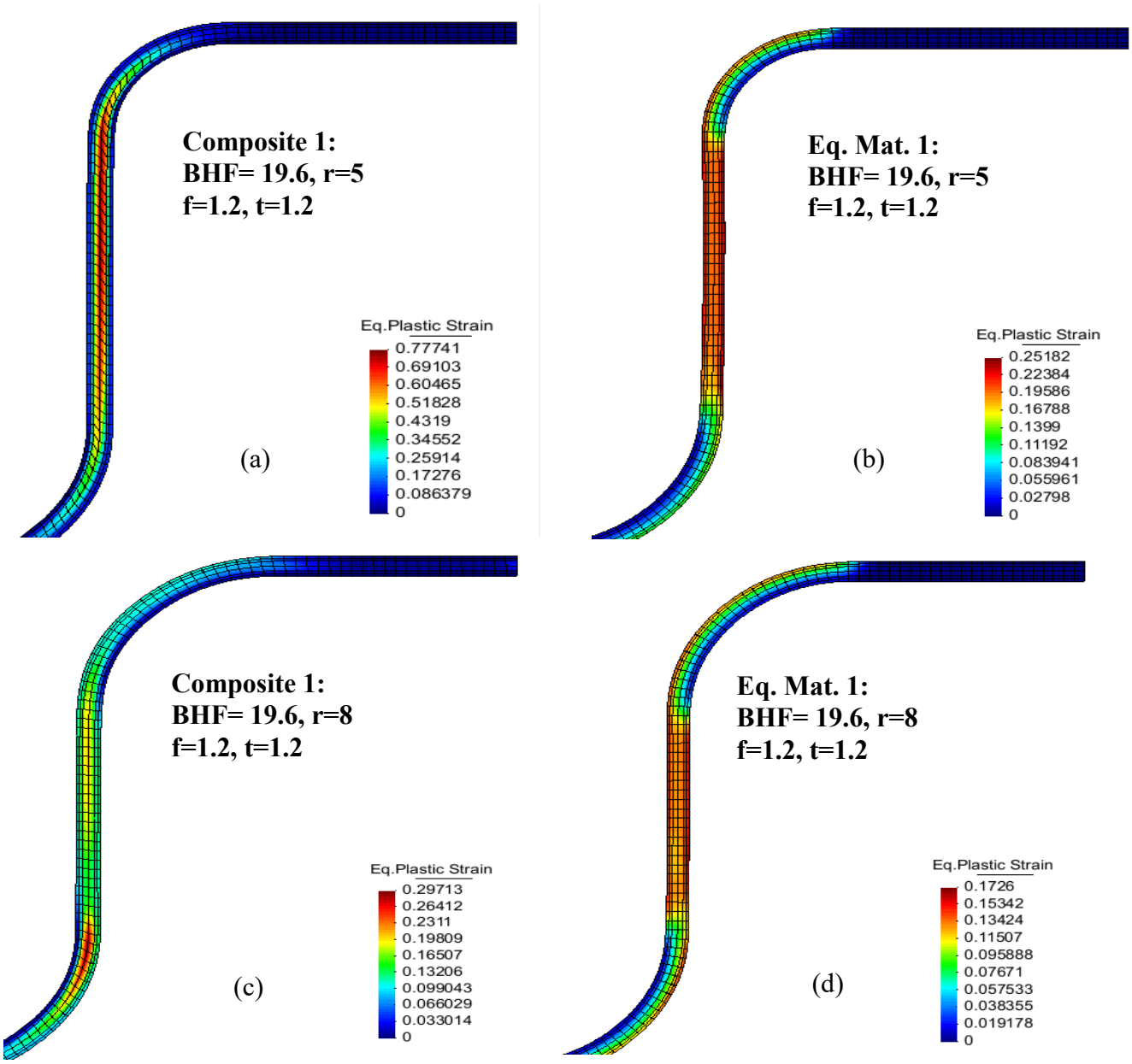

Figure 3.7. Distribution of equivalent plastic strain at the end of the forming process: (a) composite 1 – Case F; (b) Equivalent material 1 – Case F; (c) composite 1 – Case G; (d) Equivalent material 1 – Case G

In order to test the effect of the core thickness, simulations were performed with a multilayer sheet having a core 0.6 mm thick (instead of 1 mm), keeping the thickness of the outer layers. In the simulations of the composite and the equivalent material, the value of BHF is equal to 19.6 kN and the punch-die clearance is equal to the sheet thickness (f=t=1.2 mm). Two values of die radius, 5 mm to 8 mm, were used. The results are shown in Figure 3.7.

These results show that, when using a 5 mm die radius, the maximum value of the equivalent plastic strain increases with the reduction of the core thickness in the case of the composite (from 66% for thickness t = 1.6 mm to 78% for thickness t = 1.2 mm); however, it decreases for the equivalent material (from 31% to 25%). For the die radius of 8 mm, the maximum value of the equivalent plastic strain decreases for the composite and the equivalent material with the reduction of the core thickness (from 34% to 30%, in case of the composite; from 22% to 17%, in case of the equivalent material). Thus, core thickness variation does not seem decisive in the strain distribution.

3.2.2. Composite 2

Table 3.2 displays the combinations of parameters that were used for the simulations of composite 2.

Table 3.2. Combination of parameters used for the simulations of composite 2

Case	BHF [kN]	r [mm]	t [mm]	f [mm]
H	19.6	5	1.6	1.6
I	19.6	8	1.6	1.6
J	19.6	5	1.2	1.2
K	19.6	8	1.2	1.2

The blank holder force was fixed at 19.6 kN, since it proved to be more effective than BHF=4.9 kN and the punch-die clearances are equal to sheet thicknesses (1.2 and 1.6 mm); the die radius values used are equal to 5 mm or 8 mm. Thus, only the effects of the die radius and sheet thickness were analysed.

Figures 3.8, 3.9 and 3.10 show the strain distributions at the end of the forming process, for the case of composite 2 in Table 3.2. In cases of the thickness equal to 1.6 mm, the strain distributions of the equivalent material are also presented in Figures 3.8 and 3.9,

showing that the maximum strain values are equal for the composite and the equivalent material, regardless of the die radius. In cases of the thickness equal to 1.2 mm, the maximum strain value is lower than for the 1.6 mm thickness, for both die radius values, 5 and 8 mm. The influence of the die radius is qualitatively similar to that observed for the composite 1.

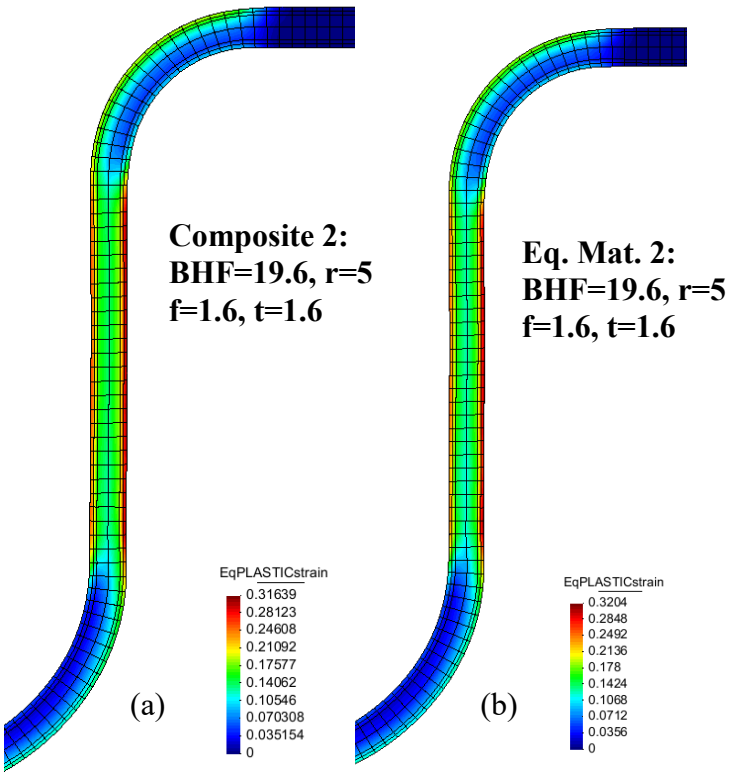

Figure 3.8. - Distribution of equivalent plastic strain at the end of the forming process (Case H): (a) composite 2; (b) Equivalent material 2

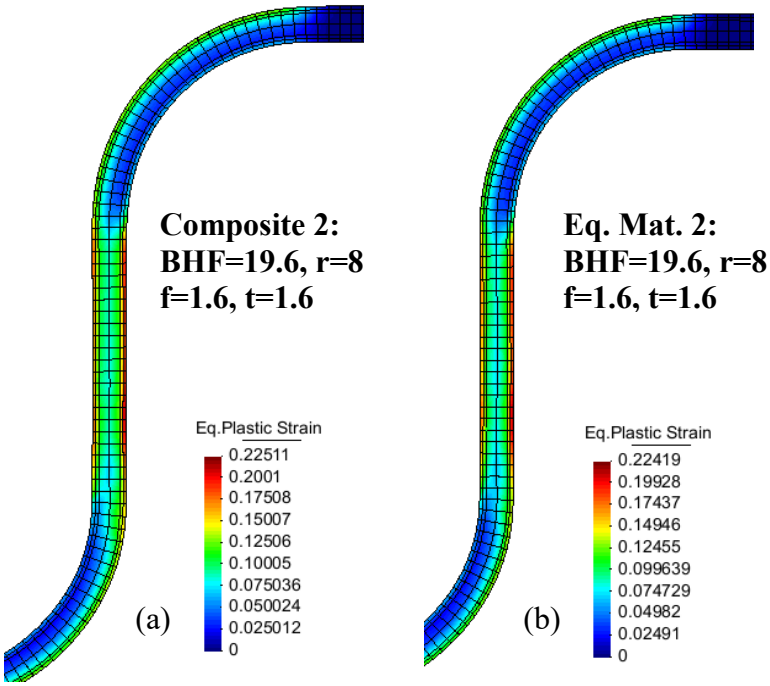

Figure 3.9. - Distribution of equivalent plastic strain at the end of the forming process (Case I): (a) composite 2; (b) Equivalent material 2

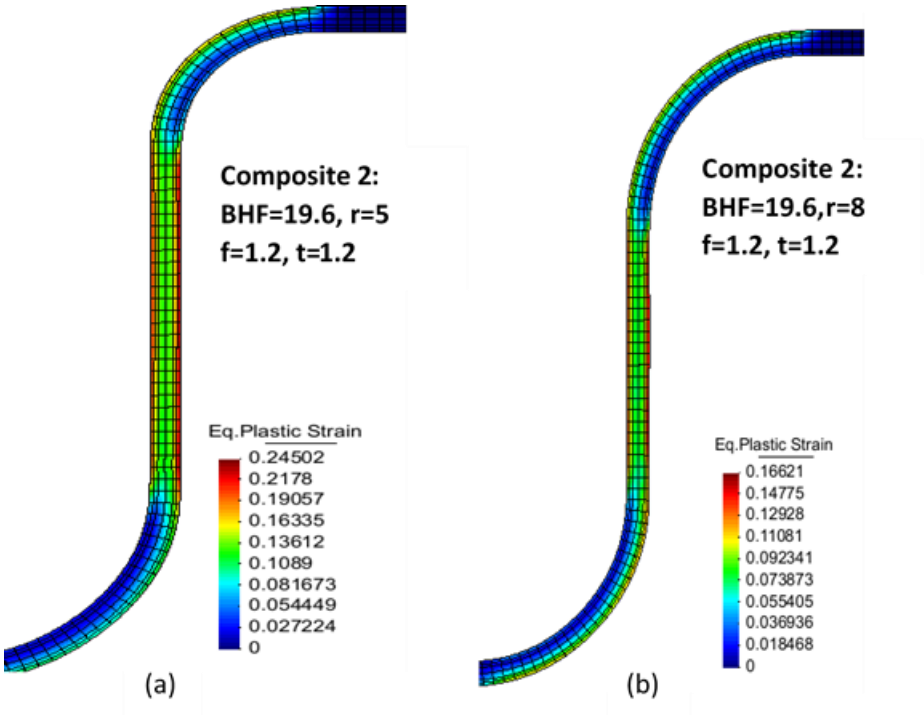

Figure 3.10. Distribution of equivalent plastic strain at the end of the forming process of the composite 1: (a) Case J; (b) Case K

In conclusion, when the difference of mechanical behaviour of the constituent materials of the composite decreases, the strain distribution of the composite approximates that of the corresponding equivalent material, as it happens for the composite 2.

3.3. Force *vs.* displacement analysis

Another point of interest of this forming process is to assess the relationship between the force and displacement of the punch. Figures 3.11 to 3.13 show the results of force *vs.* displacement of the punch in case of composite 1, for the combinations of the forming parameters A, B and E (see Table 3.1). In Case A (Figure 3.11), there are noticeable differences between the curve of the composite and that of the equivalent material, where the composite curve has a higher level. These differences can be seen as natural, since the process conditions defined for Case A lead to a strong gradient of deformation in the composite, unlike the equivalent material. The same does not happen in composite 1 when the forming conditions are as defined in Case B (Figure 3.12) and Case E (Figure 3.13), for which the curves of the composite and the equivalent material are similar.

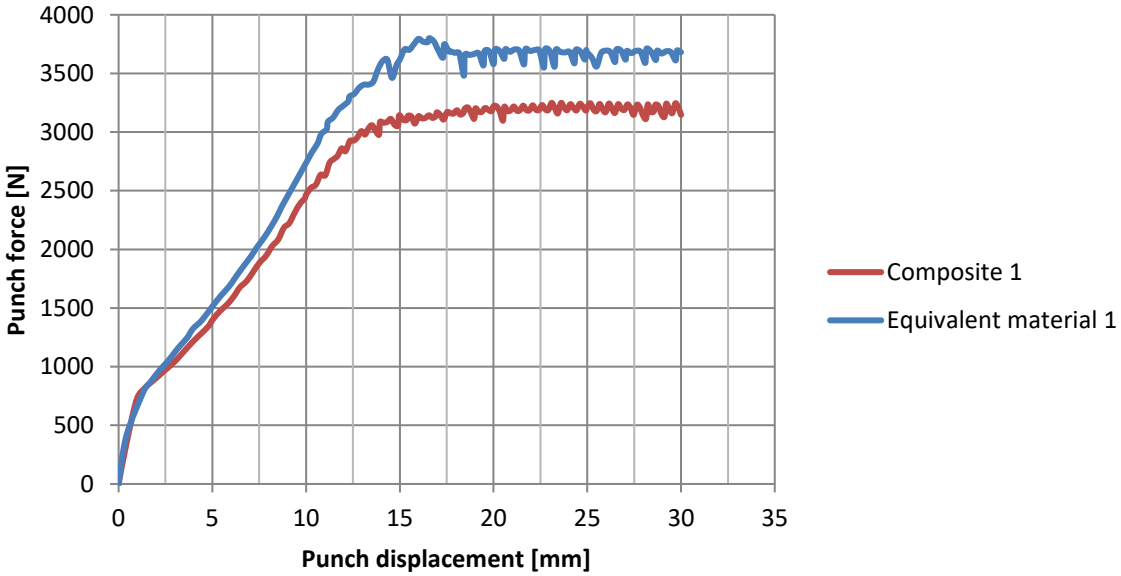

Figure 3.11. Force *vs.* displacement of the punch during the deep drawing process of the U-channel profile for the case of composite 1 (Case A).

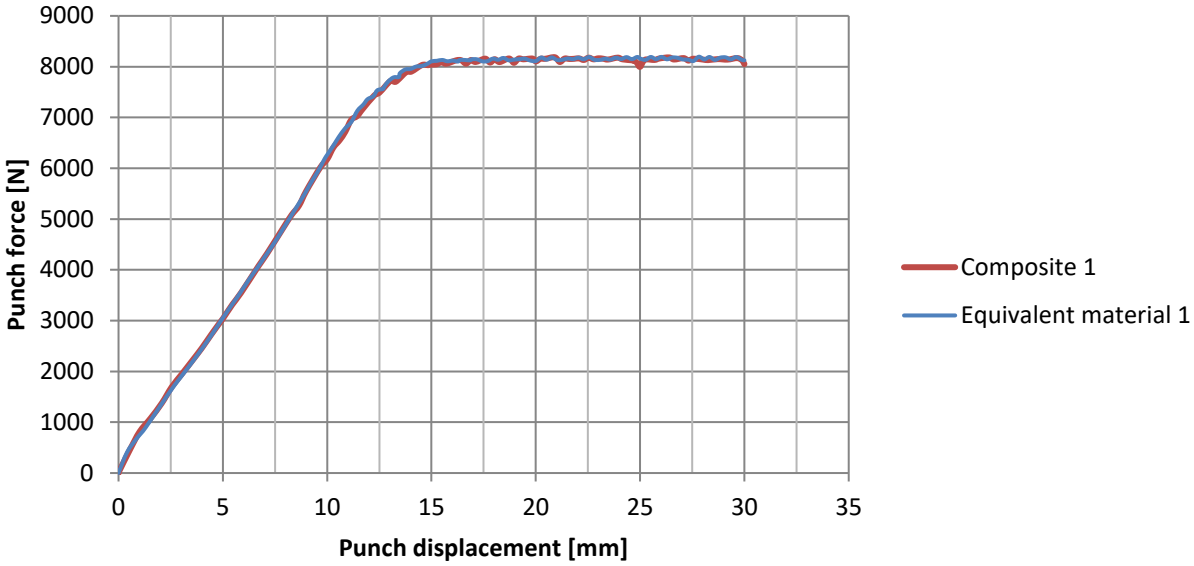

Figure 3.12. Force *vs.* displacement of the punch during the deep drawing process of the U-channel profile for the case of composite 1 (Case B).

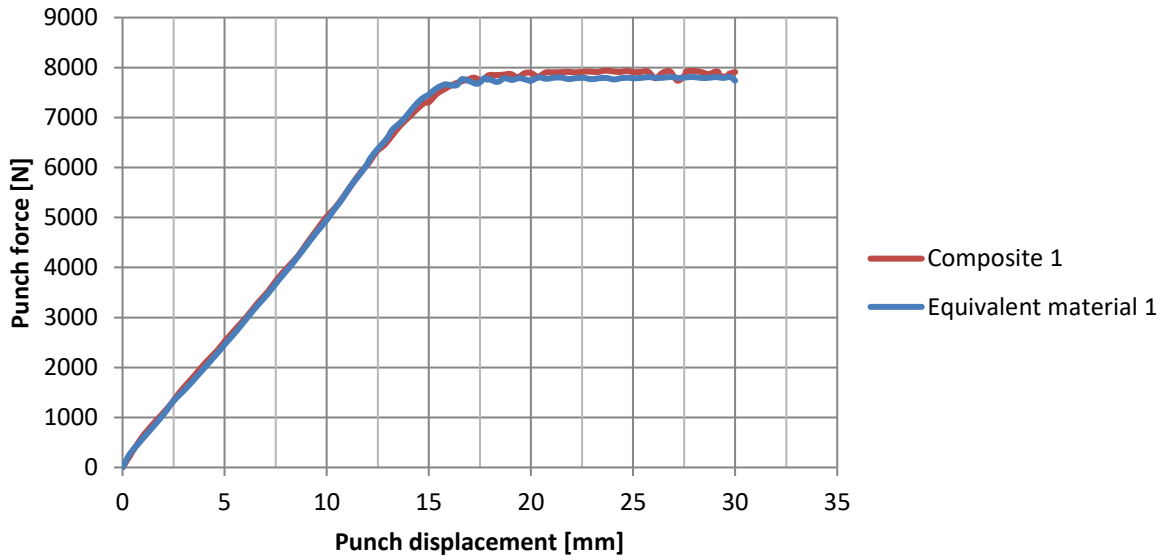

Figure 3.13. Force *vs.* displacement of the punch during the deep drawing process of the U-channel profile for the case of composite 1 (Case E).

For composite 2, the results of force *vs.* displacement of the punch are shown in Figures 3.14 and 3.15, for the cases of the combinations of the forming parameters H and I. that the level of the force to displace the punch is higher than for composite 1, since the core of composite 2 requires higher stress to deform. Moreover, the results regarding the composite and the equivalent material are very similar, since their mechanical behaviour is not so far apart.

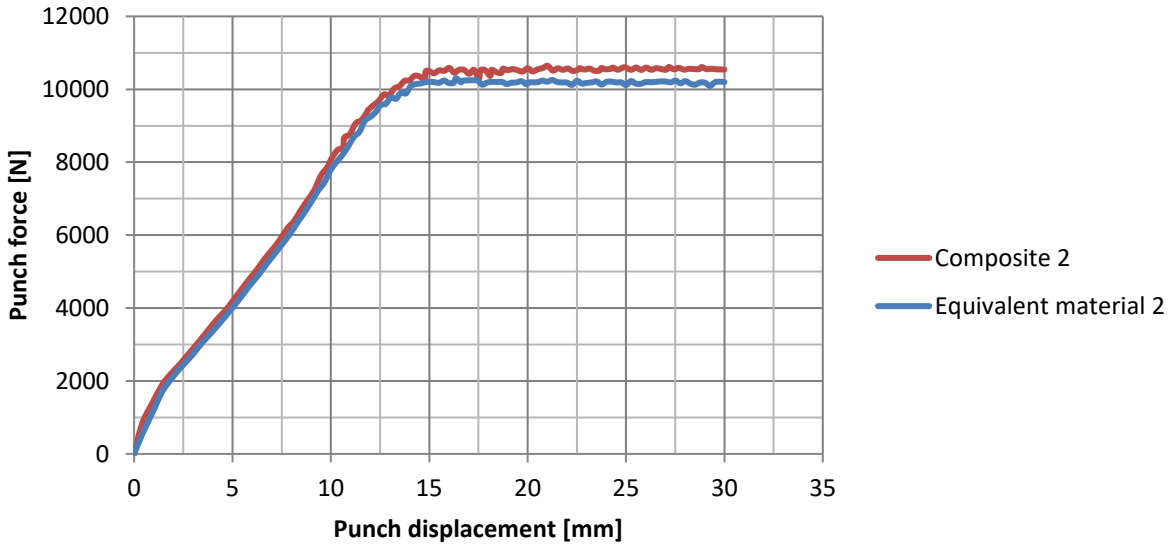

Figure 3.14. Force *vs.* displacement of the punch during the deep drawing process of the U-channel profile for the case of composite 2 (Case H)

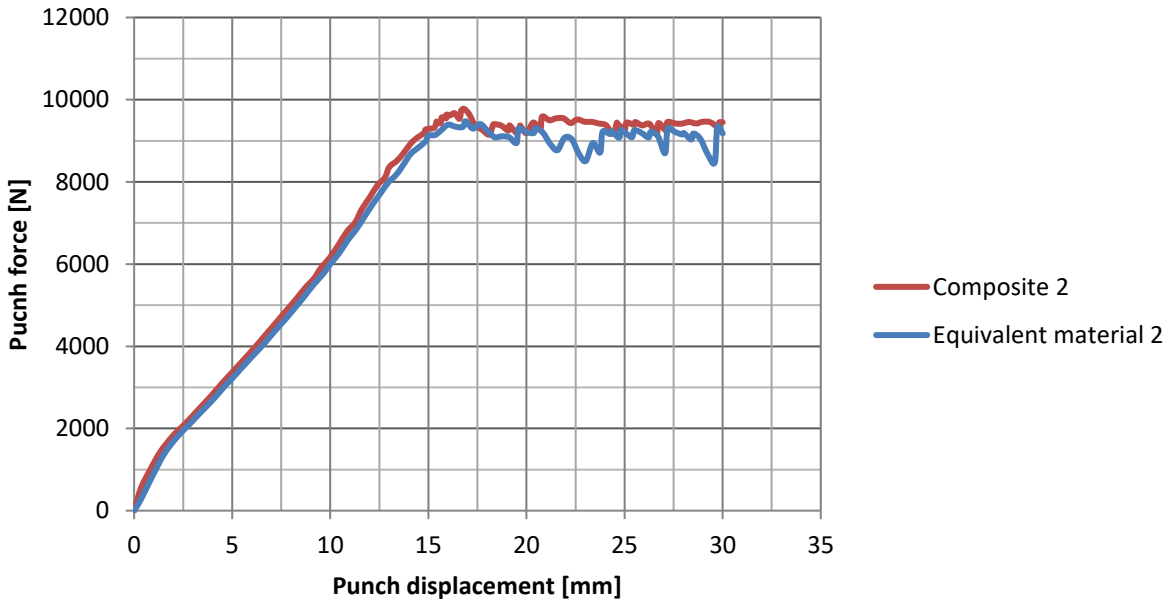

Figure 3.15. Force *vs.* displacement of the punch during the deep drawing process of the U-channel profile for the case of composite 2 (Case I)

4. DEEP DRAWING OF A SQUARE CUP

The second forming process studied in this thesis is the deep drawing of a square cup, which presents a type of symmetry different from the previous forming process.

4.1. Numerical modelling

Due to material and geometric symmetries only a quarter of the surface was considered for the simulations of the composites 1 and 2. The initial surface dimensions of the sheet were 75x75 mm. The setup is similar to the deep drawing of a U-channel profile. The die radius is equal to 5 mm and the punch radius is 8 mm. The clearance between the die and the punch is 4 mm. Two values of the blank holder force were used, as for the U-channel process: BHF = 4.9 kN and 19.6 kN. A mesh sensitivity analysis based on the evolution of the force vs. displacement of the punch was carried out in order to find the best compromise between accuracy and simulation time. Four different meshes, with 1.6 mm of thickness, were analysed: 20x20x8, 40x40x8 and 60x60x8 and 40x40x6. For the meshes with 8 elements along the thickness, the core contains four of them. Figure 4.1 shows the force *vs.* displacement of the punch, for the four meshes, in case of composite 1.

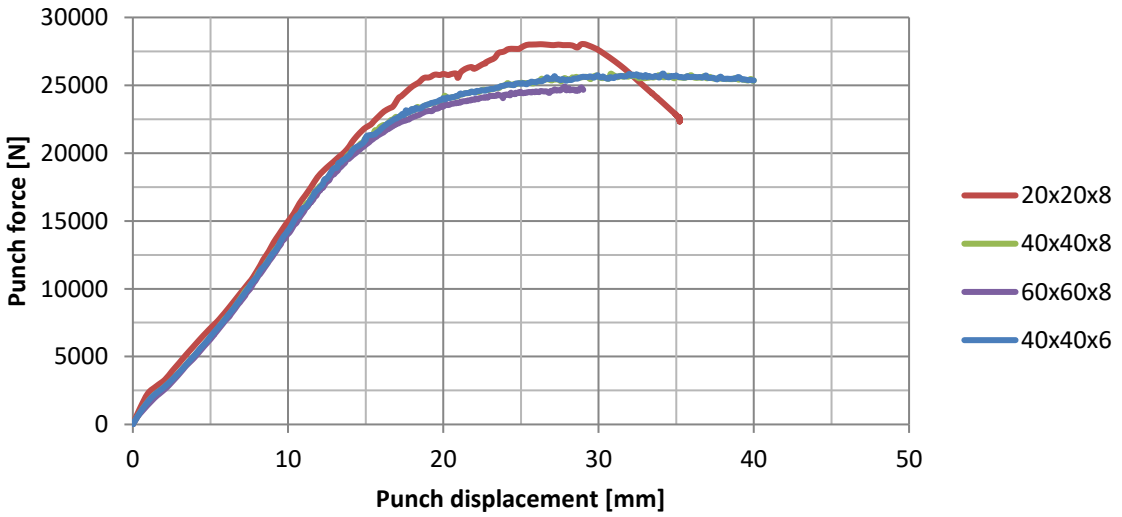

Figure 4.1. Force *vs.* displacement of the punch, for the mesh sensitivity analysis (composite 1, BHF = 19.6 kN)

Taking these results into consideration, it was decided to use the 40x40x6 mesh for the simulations, as it offered a convenient simulation time and accurate results. As for the bulge test and U-channel profile, each layer of the composite material is composed of two layers of elements. In total, the mesh contains 9600 hexahedral elements.

4.2. Strain distribution analysis

The results of the strain distributions of the two composites are presented and compared with those of the equivalent materials. Blank holder force values of 4.9 and 19.6 kN are considered.

Figure 4.2 shows that, for composite 1, the increase of the blank holder force leads to a reduction of the maximum equivalent strain value of about 15%, even though the strain values in the composite core are high, as can be seen in the vertical wall and the far right corner in the side view.

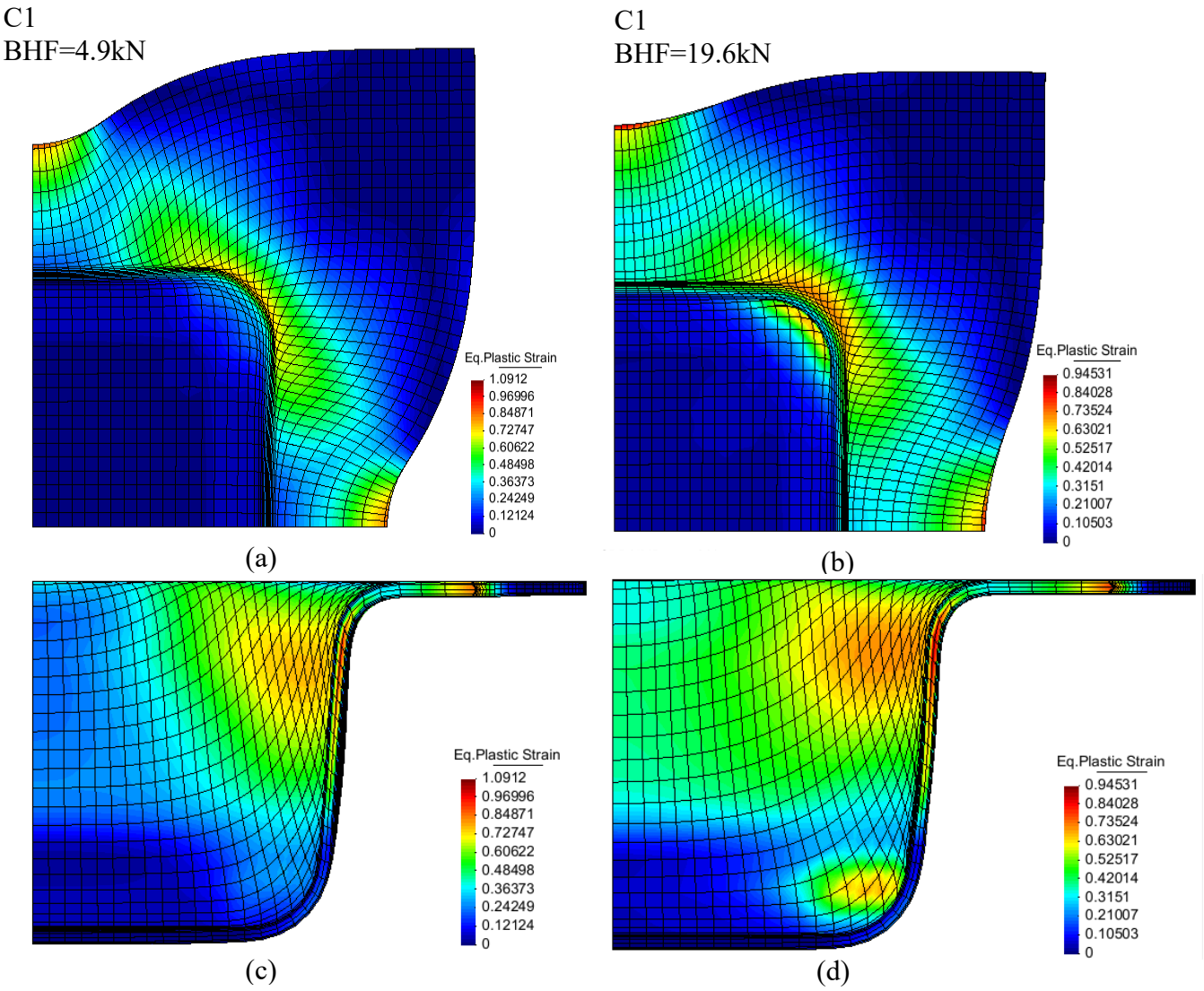

Figure 4.2. Distribution of equivalent plastic strain in the composite 1 at the end of the process for: (a) BHF=4.9 kN, top view; (b) BHF=19.6 kN, top view; (c) BHF=4.9 kN, side view; (d) BHF=19.6 kN, side view

Figure 4.3 shows the results for the equivalent material 1, in order to compare with the composite. The higher blank holder force leads to an increase in the maximum equivalent plastic strain of the equivalent material, going from 95% with BHF=4.9 kN to 108% with BHF=19.6 kN. It must be emphasized that the maximum equivalent strain occurs in distinct areas of the sheet, when comparing the composite with the equivalent material. In case of composite it occurs in the core for both values of BHF. In case of the equivalent material seems to occur in surface, although the location depends on the BHF value.

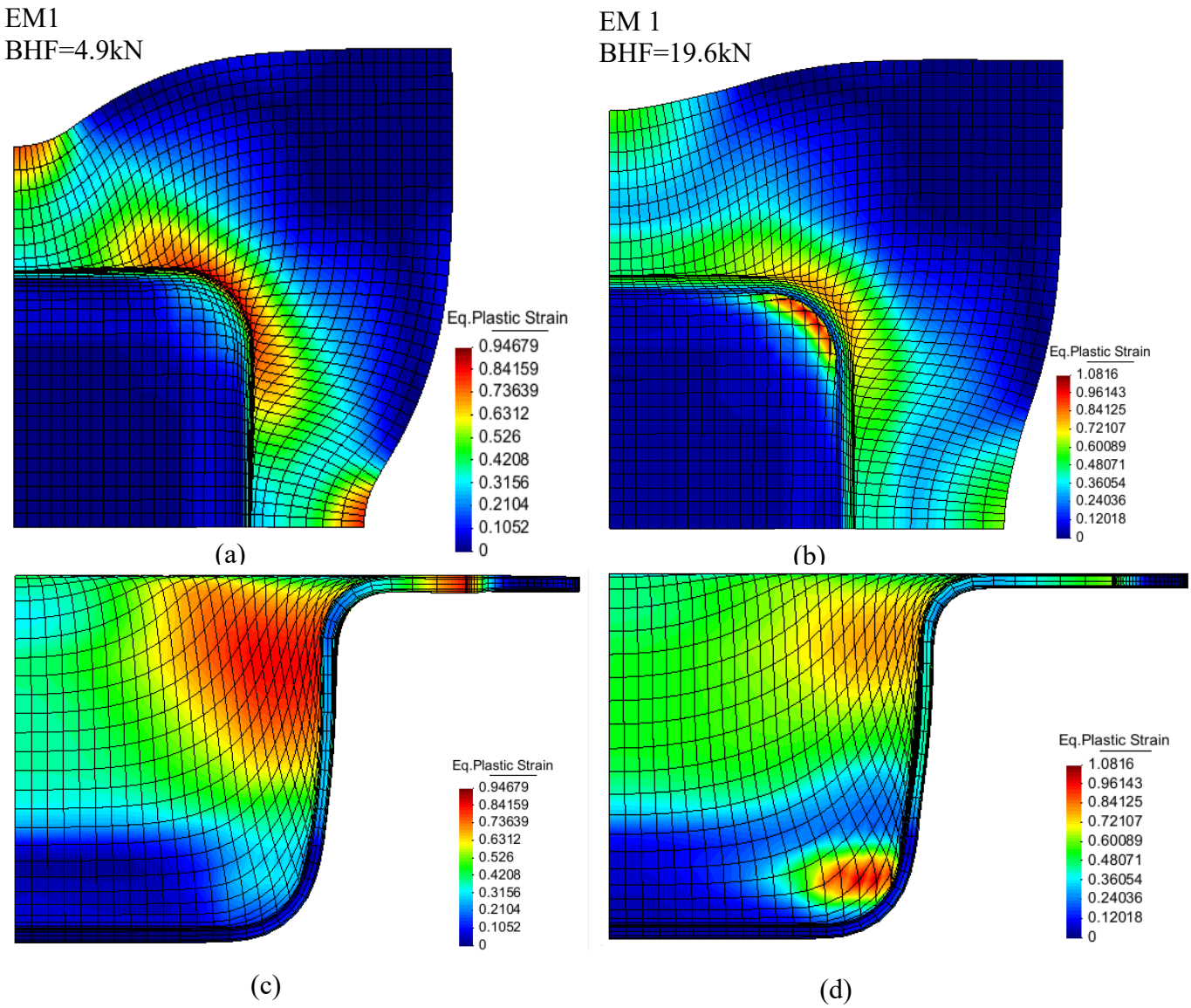

Figure 4.3. Distribution of equivalent plastic strain in the equivalent material 1 at the end of the process for: (a) BHF=4.9 kN, top view; (b) BHF=19.6 kN, top view; (c) BHF=4.9 kN, side view; (d) BHF=19.6 kN, side view

Regarding composite 2 and its equivalent material, the blank holder force does not significantly influence the maximum values of strain in both cases, as shown in Figures 4.4 and 4.5, respectively. Also, the differences between the composite and the equivalent material are not significant.

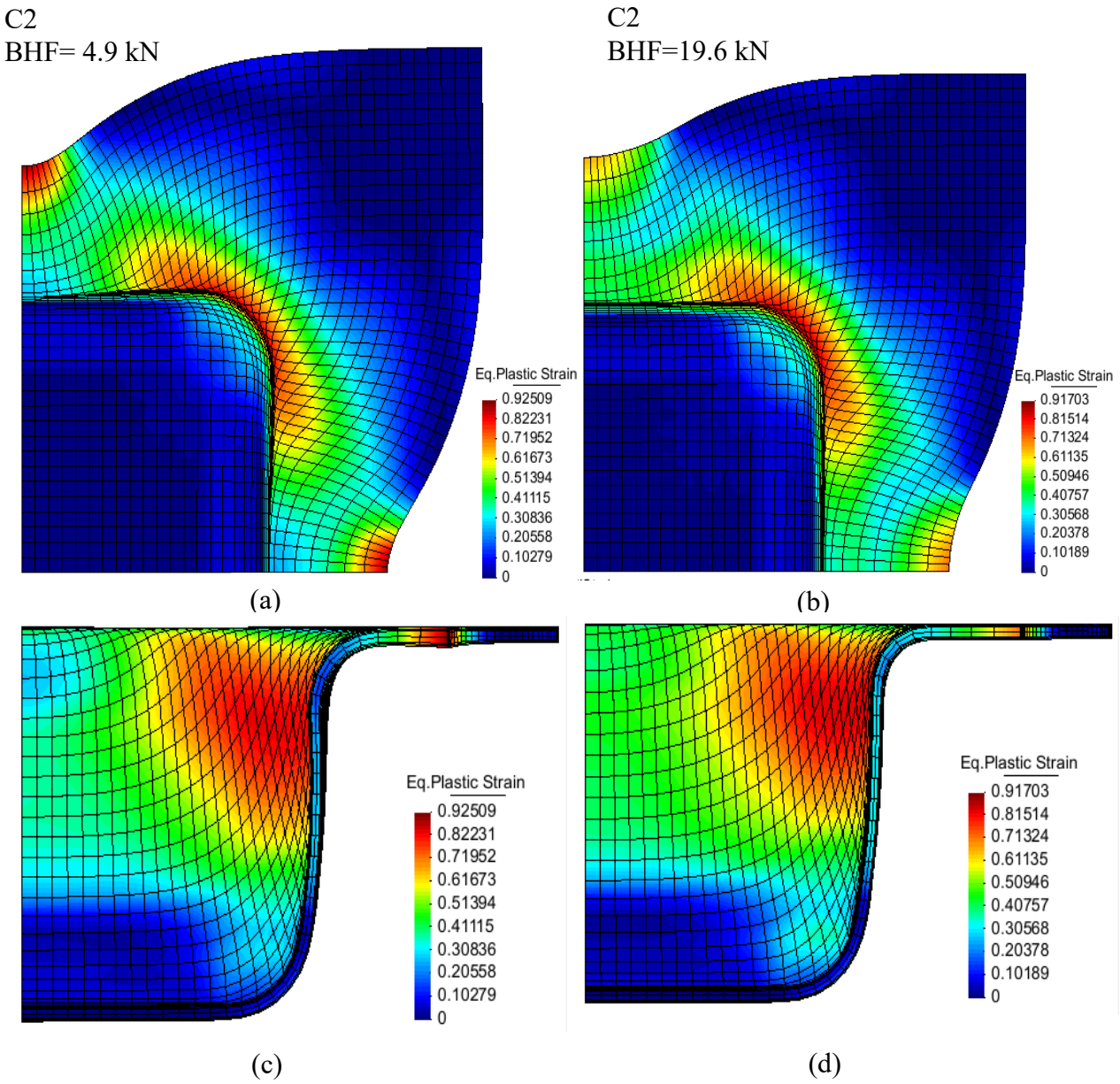

Figure 4.4. Distribution of equivalent plastic strain in the composite 2 at the end of the process for: (a) BHF=4.9 kN, top view; (b) BHF=19.6 kN, top view; (c) BHF=4.9 kN, side view; (d) BHF=19.6 kN, side view

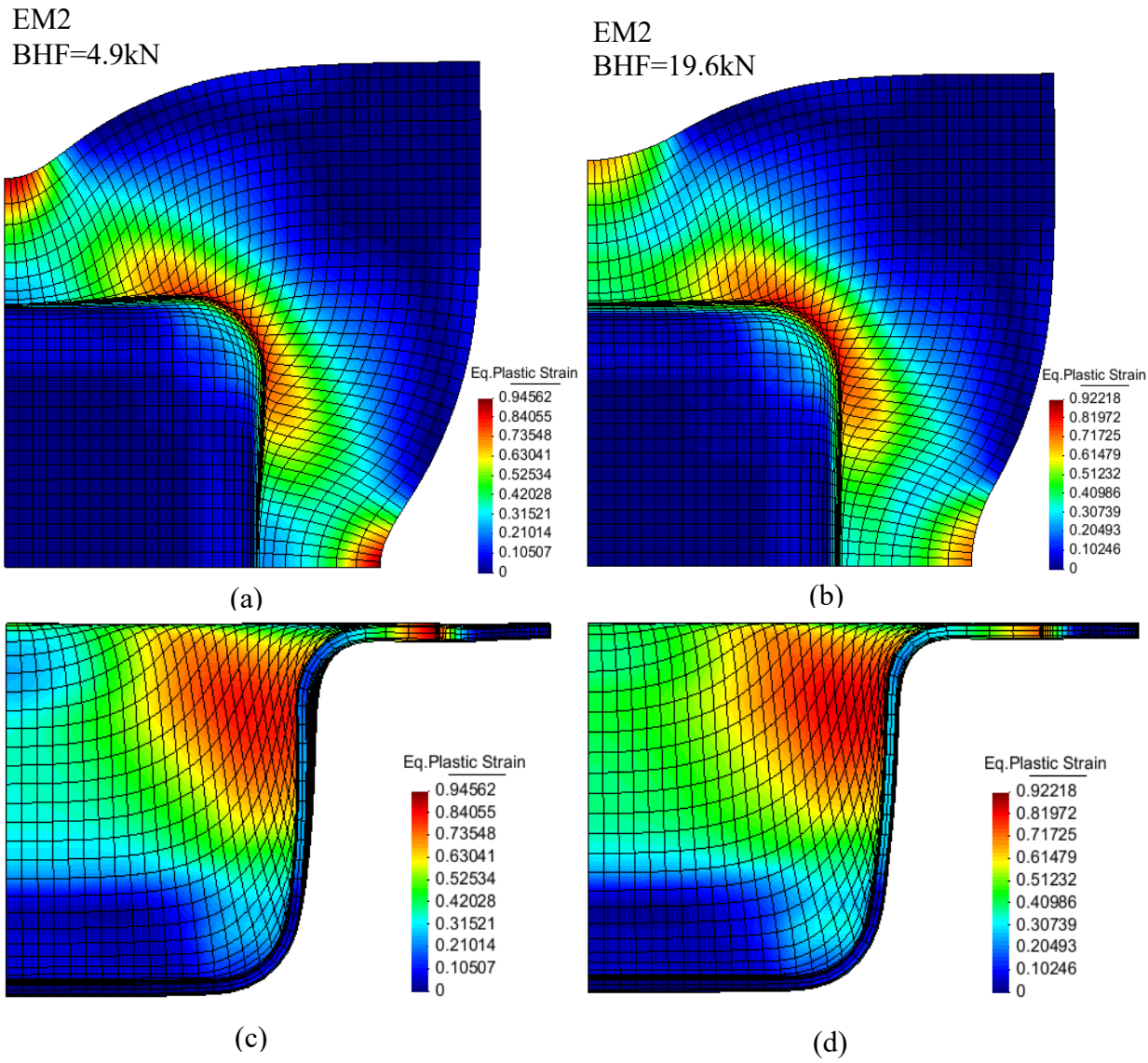

Figure 4.5. Distribution of equivalent plastic strain in the equivalent material 2 at the end of the process for: (a) BHF=4.9 kN, top view; (b) BHF=19.6 kN, top view; (c) BHF=4.9 kN, side view; (d) BHF=19.6 kN, side view

4.3. Force *vs.* displacement analysis

Similar to the deep drawing of the U-channel profile, the objective of the numerical simulations of this test is also to obtain the force *vs.* displacement results for the two composites and the two BHF values.

4.3.1. Composite 1

Figures 4.6 and 4.7 display the comparison of the curves of force *vs.* displacement of the punch for the composite 1 and its equivalent material, with BHF = 4.9 and 19.6 kN, respectively. In both cases, the curves of the composite and the equivalent material are very similar, although the match is best for BHF = 19.6 kN.

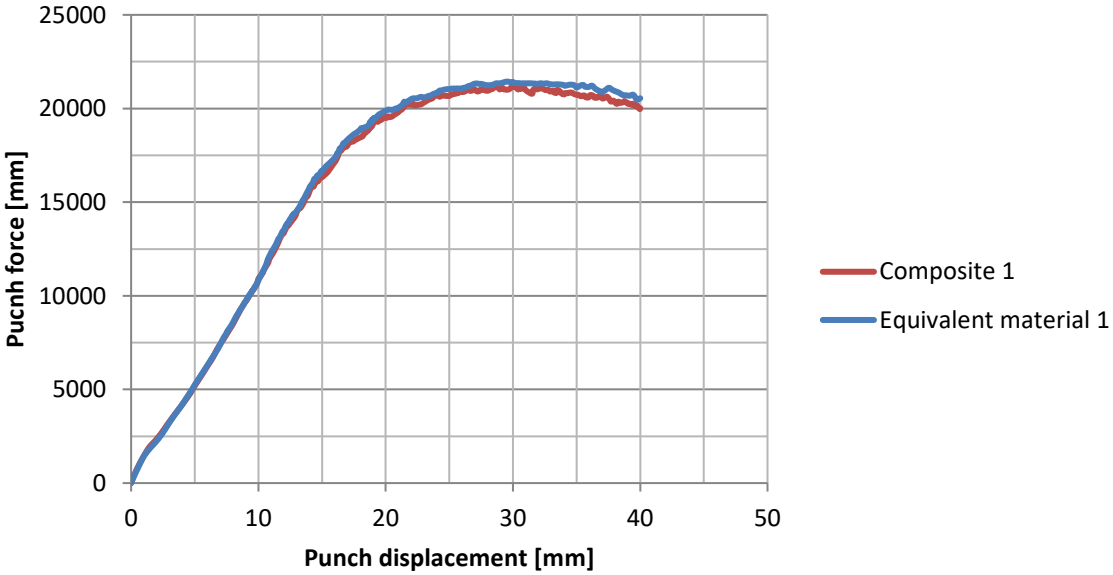

Figure 4.6. Force *vs*. displacement graphs for composite 1 and equivalent material 1 with BHF=4.9 kN

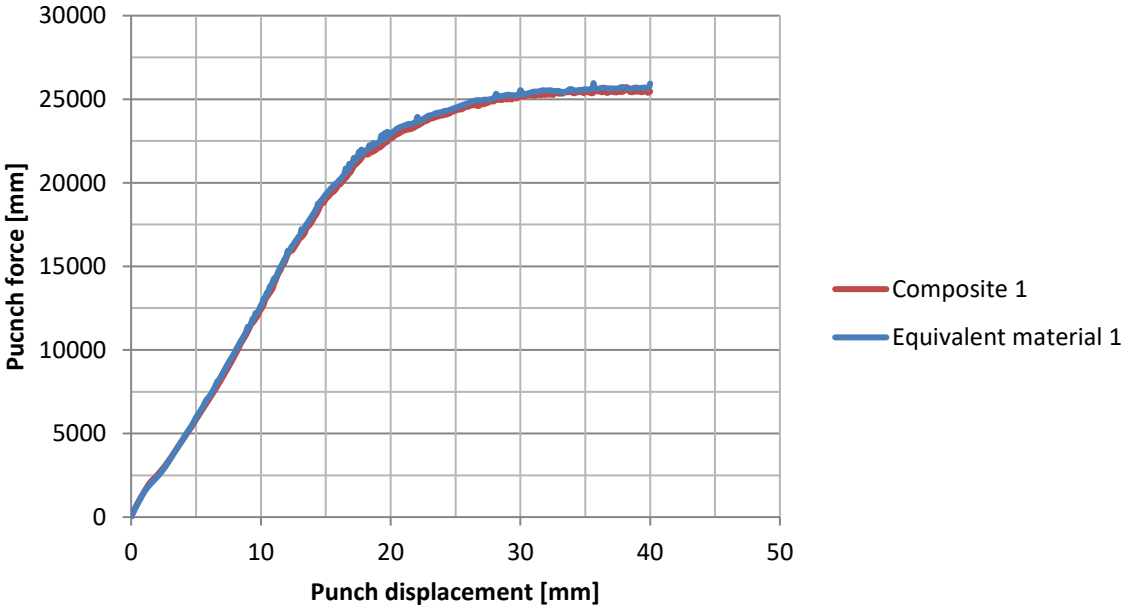

Figure 4.7. Force *vs*. displacement graphs for composite 1 and equivalent material 1 with BHF=19.6 kN

4.3.2. Composite 2

The results of force *vs.* displacement of the punch for the composite 2 and its equivalent material are shown in Figures 4.8 and 4.9, for the blank holder forces of 4.9 and 19.6 kN, respectively. The comparison between the composite material and the equivalent material reveals identical behaviours in both cases of BHF. Figure 4.9 shows the curves obtained for the same materials when BHF=19.6 kN.

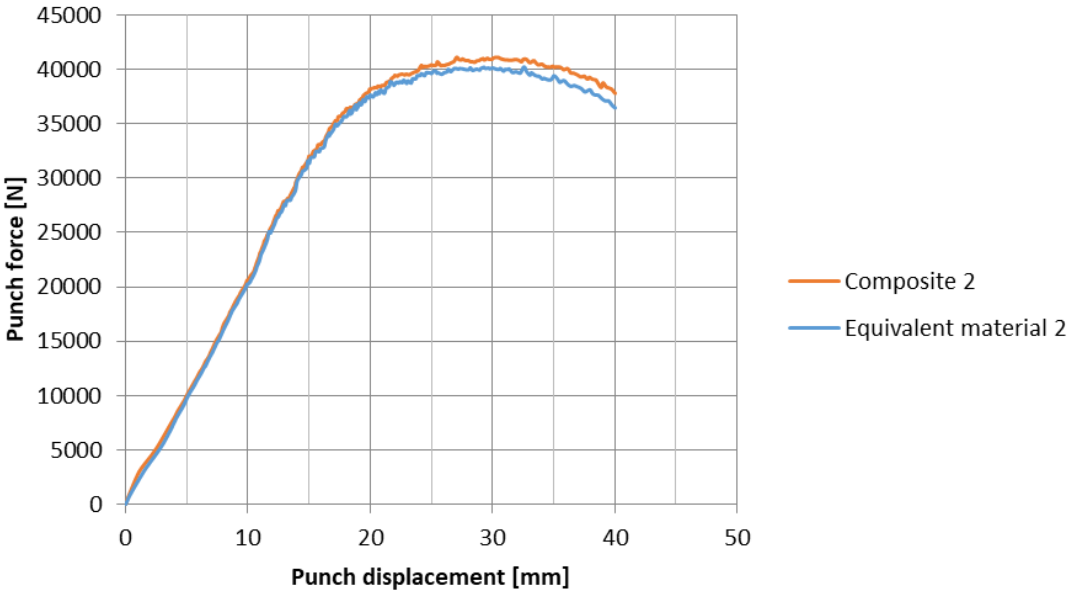

Figure 4.8. Force *vs.* displacement graphs for composite 2 and equivalent material 2 with BHF=4.9 kN

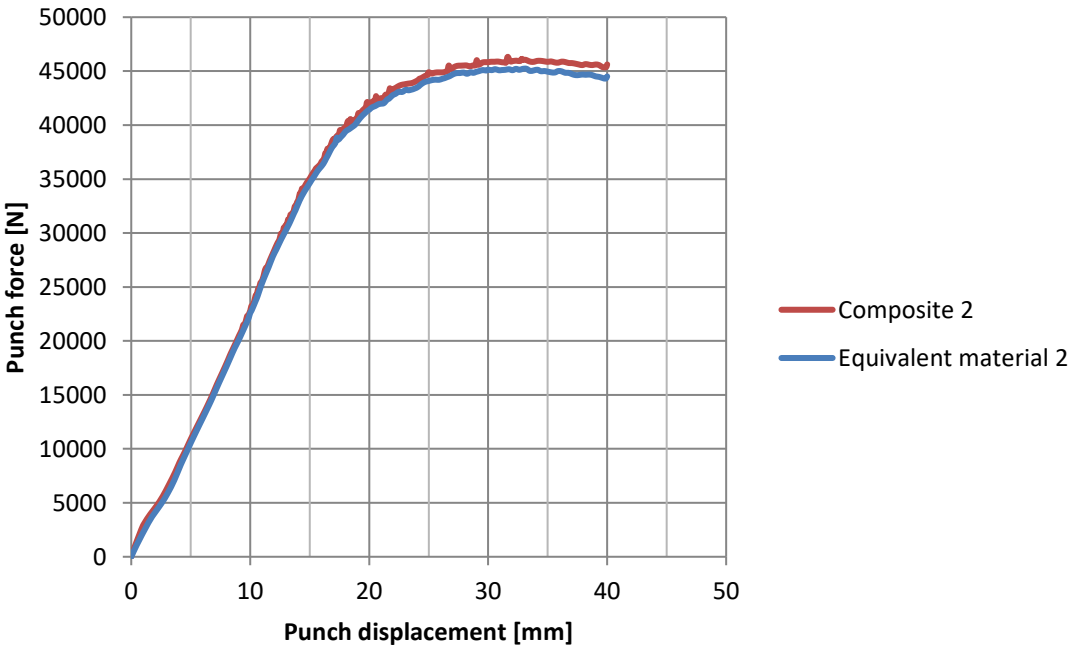

Figure 4.9. Force *vs.* displacement graphs for composite 2 with BHF=19.6 kN

5. CONCLUSIONS AND FUTURE WORK

In a world where engineering solutions demand ever-greater efficiency, composite materials are assuming an increasingly important role, since they can provide the performance of traditional materials, with a much lower weight. This dissertation describes a numerical study that aims to characterize the plastic behaviour of a composite, sandwich material, made up of two outer layers of steel and a polymeric or aluminium core. The analysis of the plastic behaviour of composite material is based on three tests/processes: the bulge test and the deep drawing processes of a U-channel profile and a square cup. Two materials, designated as composites 1 and 2, were studied. The plastic behaviour of equivalent materials were identified from the bulge test results. These materials were used for comparison during the analysis of the behaviour of the composites.

The bulge test results show that the pressure vs. pole height curve of the composite can be obtained by the weighted average of the corresponding curves of the constituent layers. The equivalent material seems to replicate well the behaviour of the composite in relation to the equivalent plastic strain; consequently, there are substantial differences between both materials with regard to equivalent stress.

Numerical simulations of U-channel profile and square cup forming process were performed in order to analyse the behaviours of the two-layered during industrial-type processes. The aim is to understand the specific forming characteristics of the three-layered materials.

Under certain forming process conditions of the U-channel profile, large plastic deformation can occur in the composite core in contrast to the outer layers, which can lead to delamination. The blank holder force seems to be the most influential in the magnitude of the strain gradient. Also, the die radius has an influence identical to that of the blank holder force. The thickness and clearance seem to have less influence.

This work allowed exploring some general issues about the behaviour of sandwich composites during deep-drawing forming processes. It will be of interest, in a next step, to analyse in detail how the deformation of these materials, which generates strong strain gradients, is related to the delamination that can occur during forming.

BIBLIOGRAPHY

Andrews E.W. and Moussa N.A., 2009. Failure mode maps for composite sandwich panels subjected to air blast loading, International Journal of Impact Engineering, 36, 418-425

Bagherzadeh S., Mollaei-Dariani B., Malekzadeh K., 2012. Theoretical study on hydro-mechanical deep drawing process of bimetallic sheets and experimental observations, Journal of Material Processing Technology, 212, 1840-1849

Harhash M., Sokolova O., Carradó A., Palkowski H., 2014. Mechanical properties and forming behaviour of laminated steel/polymer sandwich systems with local inlays – Part 1, Composite Structures, 118, 112-120

Harhash M., Carradó A., Palkowski H., 2017. Mechanical properties and forming behaviour of laminated steel/polymer sandwich systems with local inlays – Part 2: Stretching and deep drawing, Composite Structures, 160, 1084-1094

Kim J.G., Baek S.M., Cho W.T., Song T.J., Chin K-G., Lee S., Kim H.S., 2017. On the Rule-of-Mixtures of the Hardening Parameters in TWIP-Cored Three-Layer Steel Sheet, Met. Mater. Int, Vol. 23, No. 3, pp. 459-464. DOI: 10.1007/s12540-017-6674-0

Marandi F.A., Jabbari A.H., Sedighi M., Hashemi R., 2017. An Experimental, Analytical, and Numerical Investigation of Hydraulic Bulge Test in Two-Layer Al–Cu Sheets. DOI: 10.1115/1.4034717

Miranda S.C., Amaral R.L., Santos A.D., Oliveira T. F., Malheiro L. T., 2017. Análise e caracterização do comportamento de um material híbrido, aço com núcleo polimérico, CIBEM - 13º Congresso Ibero-americano de Engenharia Mecânica

Prates P.A., Adaixo A.S., Oliveira M.C., Fernandes J.V., 2018. Numerical study on the effect of mechanical properties variability in sheet forming processes, The

International Journal of Advanced Manufacturing Technology, vol. 96, issue 1-4, pp. 561-580

Santos A.D., Teixeira P., Barata da Rocha A., Barlat F., Moon YH., Lee M-G., 2010. On the determination of flow stress using bulge test and mechanical measurement, Proceedings of the 10th International Conference on NUMIFORM. American Institute of Physics Pohang, Republic of Korea, p. 845-852

Sokolova O.A., Carradò A., Palkowski H., 2011. Metal–polymer–metal sandwiches with local metal reinforcements: A study on formability by deep drawing and bending, Composite Structures 94, 1-7